Collision, mantle convection, and Tethyan closure in the Eastern Mediterranean

Eivind O. Straume[1,4,†], Claudio Faccenna[2,3], Thorsten W. Becker[4,5], Bernhard Steinberger[2], Alexis Licht[6], Andrea Sembroni[3] , Zohar Gvirtzma[7,8], Paolo Ballato[3]

†**e-mail:** eist@norceresearch.no

[1] *NORCE Norwegian Research Centre & The Bjerknes Centre for Climate research, Bergen, Norway.*

[2] *GFZ Helmholtz Centre for Geosciences, Potsdam, Germany*

[3] *University of Roma TRE, Dept. of Science, Rome, Italy*

[4] *University of Texas Institute for Geophysics (UTIG) & Department of Earth and Planetary Sciences (EPS), Jackson School of Geosciences, University of Texas at Austin, Austin, TX, USA*

[5] *Oden Institute for Computational Engineering & Sciences, University of Texas at Austin, Austin, TX, USA*

[6] *Aix-Marseille Université, French National Centre for Scientific Research (CNRS), French Research Institute for Development (IRD), French National Research Institute for Agriculture, Food and the Environment (INRAE), Centre de recherche et d'enseignement de géosciences de l'environnement (CEREGE), Aix-en-Provence, France*

[7] *Geological Survey of Israel, Yesha'yahu Leibowitz, Jerusalem, Israel*

[8] *Institute of Earth Sciences, The Hebrew University of Jerusalem, Jerusalem, Israel*

Abstract

The Tethys Seaway once linked the Atlantic and Indo-Pacific oceans. Its gradual shallowing and closure impacted global ocean circulation, faunal diversification, and climatic changes. In this Review, we evaluate the tectonic causes and the topographic changes across the Eastern Mediterranean over the last 66 Ma and explore the consequences of Tethys Seaway closure. Mantle convection led to collisional tectonic processes, mountain building and crustal thickening along the Tethyan realm. The Ethiopian flood basalts mark the arrival of the Afar Plume at ~ 33 - 28 Ma, followed by northward-trending volcanic activity indicating that plume material had moved to northwest Arabia by ~20 Ma. Plume-induced mantle flow generated kilometer scale uplift across

East Africa, at ~8°N at ~35 Ma, and along Arabia, and led to the formation of the *Gomphotherium* land bridge at 30°N, ~20 Ma. Afro-Arabian uplift contributed to the development of modern-like Asian monsoons and the land bridge between Africa and Asia enabled one of the greatest faunal interchanges of the Cenozoic. The gradual shoaling and final closure of the Tethys Seaway likely facilitated the transition toward a stronger overturning circulation in the North Atlantic, contributing to the Cenozoic cooling trend. Future research should focus on understanding the connection between mantle dynamics and surface process, and exploring the possible impact on the biosphere and climate.

Website Summary:

Closure of the Tethys Seaway marked the last connection between the Atlantic and Indo-Pacific oceans. This Review explores how mantle convection and associated volcanic activity caused Tethys Seaway closure and discusses the implications for ocean circulation, faunal diversification, and climate.

Key points

1. Mantle convection driven tectonics produce a distinct dynamic topography high stretching from East Africa northward.
2. Convection and associated volcanic activity controlled the formation of the Eastern Mediterranean land bridge leading to the final closure of the Tethys Seaway.
3. Land bridge formation enabled the Great Old World Biotic Interchange in the Early Miocene.
4. Closure of the Tethys Seaway may have facilitated a stronger overturning circulation in the North Atlantic Ocean.
5. Tethyan paleogeography impacted the development of the modern Asian monsoons.

Introduction

The Arabia-Eurasia continental collision closed the Neothethys Ocean, ending the oceanic transport between the Indian and Atlantic Oceans through the Tethys Seaway. The collision was governed by plate tectonics and mantle convection, and had profound impacts on ocean circulation, biogeography and the climate system beyond the Eastern Mediterranean – Tethyan realm.

The Tethyan Belt (also known as the Alpine-Himalaya belt) is an area of orogenic activity encompassing the mountain ranges from the western Mediterranean to the Himalayas in the east (Fig.1, Box 1), driven by subduction and continental collision. During the subduction of the Tethys Ocean the African Plate has been slowly approaching Eurasia since the Late Cretaceous ~100 (Ma), and has been uplifted and thinned by mantle plumes which contributed to the fragmentation into continental blocks. The continental blocks consist of Adria (Alpine Mediterranean orogeny), Arabia (Bitlis-Zagros-Caucasus-Alborz) and India (Karakoram-Himalayan-Tibet). These continental blocks drifted apart from Africa at different times and moved northward toward the Tethyan subduction zone, colliding, and ending up amalgamated with Eurasia [1-4]. Adria separated from Africa in the Late Jurassic but remained kinematically linked to Africa as a promontory until at least the last million year. India separated from Africa in the late Cretaceous (~90 Ma), and Arabia lastly starting in the Late Oligocene (~25 Ma) [2,5,6]. The process leading to the separation of those blocks from Africa involves mantle upwellings, at least in the case of Arabia and India, as indicated by likely associated large igneous provinces, the Afar and Deccan flood basalts, respectively [7,8].

There are now information on the tectonic, geodynamic, and climatic history of this region[9-13]. As well as the regional paleogeographic importance in influencing large scale biogeographic dispersals[14] and even impacting human evolution by providing migration routes for early anthropoid primates[15].

In this Review, we explore the tectonic and geodynamic processes that caused the closure of the Tethys Seaway and discuss the implications for ocean circulation, faunal diversification, and climate. We focus on the formation of the Tethys collisional belt, particularly in Arabia and the Middle East, as the separation of Arabia from Africa is relatively recent (~25 Ma) [16,17]., and collision is ongoing. We begin by evaluating the tectonic and geodynamic evolution of the Mediterranean-Tethyan realm, followed by the relative role of tectonics, volcanism, and mantle convection in the closure of the Tethys Seaway. Lastly, we explore the impact on biogeography and Cenozoic climate evolution.

Africa - Arabia tectonic evolution

Africa and Arabia were connected in the early Cenozoic, until rifting in the Red Sea and Gulf of Aden led to separation by the Miocene. Concurrently, Arabia's northward motion and collision with Eurasia caused major crustal deformation, volcanism, and plateau uplift. These tectonic processes ultimately closed the deep oceanic part of the Tethys Seaway.

[H2] Africa – Arabia separation

To understand the history of Arabian plate motion, we need to reconstruct its evolution in the early Cenozoic, before continental collision, around ~50 to 40 Ma. At that time, Arabia was still part of Africa and separated from Eurasia by the Neotethys Ocean, with the oceanic lithosphere subducting northward along the Bitlis-Zagros, Aegean, and Cyprean trenches [1,2,5,13]. Africa-Arabia was progressing at a speed of about ~2-3 cm yr-1 relative to Eurasia in a north-northeasterly direction [18].

The separation of Arabia from Africa started with the formation of the Gulf of Aden and Red Sea rift systems at the beginning of the Oligocene [16,19,20]. However, full separation at a mid-ocean ridge did not start until the Miocene, at ~17 Ma in the Gulf of Aden[16] and at ~13 -12 Ma in the Red Sea[17]. The northward movement of Arabia as a single plate was accommodated by the development of two transform plate boundaries: the Dead Sea Fault to the west [21] and the Owen Fracture Zone to the east [22].

Along the margins of the Red Sea, dykes and basaltic floods were emplaced during the Oligocene [19,20], and syn-rift deposits accumulated from the Oligocene–Miocene (~30–25 Ma) to Miocene (14 Ma) [18,23]. Thermochronology shows that uplift of the Red Sea rift shoulders commenced at ~29-26 Ma and peaked at ~20 Ma [20]. Continental rifting at the Gulf of Aden is likely older, between 38 and 33 Ma [24-26], concurrently with, or slightly earlier than the onset of the Arabia-Eurasia collision.

Volcanism in Ethiopia slightly predates extension, starting at ~40-45 Ma [27], but with a climax during the Oligocene formation of the Ethiopian flood basalts [28], which covered parts of Ethiopia, Eritrea, southern Sudan, and western Yemen (Fig.1) with the emplacement of 1 million cubic kilometers of lava by 31–29 Ma [29]. The emplacement of this large igneous province was accompanied by the development of a regional truncation surface extending from the northern Red Sea to the southern Levant region related to the formation of a crustal dome, ~3000 km - 1500 km in radius, above the Afar plume [30-33].

Intraplate Volcanism is also present in Arabia with large basaltic effusions and within the collisional zone (Eastern Anatolia), with an overall progressive northward younging trend [34-37] (Figs.1 & 2, Box 1). Volcanism in Arabia at Harrat Ash Shamah (HAS) and in northwestern Syria began ~25 Ma ago [34,35], and has continued intermittently since then. The change in geochemical signature in eastern Anatolia around ~10 Ma has been also connected with the arrival of a new source of hot mantle material within the collisional zone [36-38].

[H2] Arabia – Eurasia collision

The onset of the Arabia-Eurasia collision is controversial and probably includes an inital phase of "soft" collision, which is characterized by a transition from subduction of oceanic lithosphere to thinned continental margin, followed by a "hard" one, with the arrival of thick continental crust. Collision is likely to be diachronous, with an overall eastward younging trend [39]. It is considered to have occurred sometime between the late Eocene [39-43] and the early Miocene [3,44,45], although newer studies indicate that by the middle Oligocene (~ 28-26 Ma), the Neotethys oceanic lithosphere had been subducted, placing the Arabia passive margin and its cover of obducted late Cretaceous ophiolites in the foreland position [46-48]. Between 30–35 Ma and ~20 Ma, collisional deformation was very limited and mostly localized in proximity of the plate suture [42] and along the northern edge of the collision zone, around the southern Caspian Sea rigid block [39]. Meanwhile the subduction velocity decreased progressively from ~3 to 1.5-2.0 cm yr-1 because the trench stopped retreating and started advancing [49]. Regardless, shortening increased across the entire collision zone by 20 Ma, leading to the accretion of the Arabian passive margin to the upper plate with the formation of the High Zagros, the Zagros Fold and Thrust Belt, and the Bitlis mountains [3,40,42,50]. The shortening was accompanied by the gradual thickening of the crust with maximum values of up to 70 km beneath the suture zone [51,52], and extensive upper plate deformation with the inversion of Meso-Cenozoic extensional basins along the northern sectors of the collision zone from the central Pontides in Turkey to the Kopeh Dagh in eastern Iran [39,53-55].

The collision was also associated with large-scale surface uplift, leading to the formation of the second largest collisional plateau on Earth after Tibet, the Anatolian-Iranian plateau that extends from central Anatolia to southeast Iran [56]. Overall, upper plate shortening is expected to be on the of order of ~300 km [49], although a substantial fraction of plate convergence could have been locally accommodated by intraplate subduction processes beneath the Caucasus [57] and along its eastern continuation in the central Caspian Sea Apsheron Balkhan Sill; [58]. Additional mechanisms that accommodated collisional deformation are oroclinal bending across different rigid crustal blocks forming the northern margin of the collision zone [59,60] and the lateral extrusion of Anatolia

along the North and the East Anatolian faults from the late Miocene [61-63]. Finally, during the early collision stages in the Oligocene, a pronounced phase of backarc extension initiated in the Aegean due to trench retreat, which is slab rollback in an absolute, lower mantle reference frame [1,64,65].

Those constraints indicate that the separation of Arabia from Africa and the origin of new oceanic lithosphere occured during an ongoing collisional process to the north. In addition, the northward velocity of Arabia motion surprisingly remained roughly constant, regardless of the ongoing collision which probably produced an increase in resisting forces, and the lack slab pull forces [66,67]. Its present-day motion, as derived from GPS (Fig.1, Box 1), does not differ from the plate tectonic estimate of motion since the early Miocene [18].

[H2] Closing the deep gateway

The arrival of the stretched continental passive margin of Arabia at the Eurasian trench instigated the closure of the deep oceanic gateway, perhaps as early as the late Eocene [1,68]. Marine conditions just south of the plate boundary could have persisted until the Early Miocene [45,69], though there was likely no continuous deep marine gateway after this time (Fig. 3). However, an intermediate-shallow seaway crossed the Arabian continent during the Oligocene and early Miocene, connecting the Indo-Pacific and proto-Mediterranean oceans. This seaway is sometimes referred to as the Mesopotamian Trough and allowed shallow water throughflow between the nascent Mediterranean Sea and the Indian Ocean. This epicontinental seaway acted as an efficient biogeographic barrier hindering mammal exchange between Afro-Arabia and Eurasia [70]. That seaway eventually closed in the late early Miocene (~19 Ma) with the emergence of the *Gomphotherium* land bridge, named after the iconic proboscideans that reached Asia from Africa at that time [70,71]. While the major land bridge is thought to have remained in place, there are geological indicators for a re-opening of a shallow seaway in the Mid Miocene (~16 - 12 Ma) across Arabia [9,72-74]. A similar marine connection might have existed across the upper plate in periods from the Oligocene to the early Miocene. This epicontinental sea, known in Iran as the Qom Sea, marks an episode of regional subsidence that occurred across the entire collision zone, possibly due to dynamic subsidence induced by slab and/or deep mantle dynamics [49].

The separation of Africa and Arabia and the subsequent collision with Eurasia altered regional geography and closed the deeper part of the Tethys Seaway. However, regional topographic evolution, Arabia plate motion, and closure of the epicontinental seaway across Arabia was ultimately driven by mantle convection and corresponding dynamic topography (see below) which fundamentally impacted the geography of the Middle East and beyond.

[H1] Mantle convection and the Afar Plume

Mantle convection has driven and modified surface processes in the Tethys region. We explore both the theoretical underpinnings of mantle convection and the numerical modeling methods that could unravel its impact on regional uplift, volcanism, and tectonic reconfiguration.

[H2] Mantle convection-surface tectonic links

The Mediterranean-Middle East-Horn of Africa is a promising area to explore the connections between mantle convection and surface tectonics. Here, subduction and collision are flanked by a large-scale upwelling and large igneous province emplacement which has influenced the evolution of the region. Previous efforts illustrate that the mantle has a dominant role for tectonics in this scenario [38,75-80].

The general dynamics of plate tectonics as part of mantle convection can be explored, for example, by capturing Earth's complexities such as temperature-dependent viscosity and the role of phase transitions in generic numerical models. Such computations can provide general insights into heat and mass transport rates and typical convective scenarios, such as the controls on slab avalanching and subduction triggering plumes at the core mantle boundary [81-83]. However, when exploring the details of tectonics or specific contributions to surface topography in settings like the Eastern Mediterranean, then global mantle circulation computations that incorporate seismological and other constraints are advantageous.

Mantle circulation models solve the equations of conservation of mass and momentum, and predict velocities and stresses for any type of plate boundary configurations and internal density and viscosity distributions [84-86]. Density anomalies can be inferred from Wadati-Benioff zone delineated slabs, or throughout the mantle from scaled seismic velocity anomalies in mantle tomography [85-89]. While compositional anomalies and imaging issues complicate such interpretation, away from the cratonic lithosphere at the surface or the lowermost mantle's thermo-chemical anomalies, shear wave tomography of the mantle is, to first order, dominated by temperature anomalies. Mantle rheology is complex but absolute, average upper mantle viscosities can be inferred from global isostatic adjustment and laboratory constraints, for example, and lateral and depth variations of

viscosity can be inferred from the given temperature anomalies and matching geophysical constraints such as the geoid [90-92]. The assumptions inherent in constructing such mantle circulation can then be tested further using several independent constraints, including plate velocities, total heat transport, and the match to seismic anisotropy [84,93-98].

There are trade-offs in such modeling. For example, the sinking (Stokes) velocity of an anomalously dense slab within the mantle, or the velocity of the plate it is being connected to, is given by the ratio of density anomaly and viscosity, and both properties are only known within uncertainties. However, combination of a range of constraints allows building consistent models. For example, the stress-related quantities of the geoid or dynamic topography will, to first order, not change if mantle viscosity changes by a constant factor everywhere, which provides an opportunity for joint inversion [88,99,100]. The current generation of mantle circulation models can fit both the geoid and plate velocities well for simple mineral physics motivated scalings of tomography, as long as an increase of viscosity from the upper to the lower mantle, and a relatively strong lithosphere is included[101-105].

With the background of having confidence in such large-scale geodynamic background, or "reference", models, one can then move to explore regional mobile belts, for example the Afar-Arabia-Anatolia system presented below, and test the role of different contributions such as active upwellings compared to regional slab pull for driving plate and microplate motions, generating dynamic topography, or for explaining the seismic anisotropy signal seen in *SKS* splitting (Fig. 1c) from mantle shear [37,78,89,106,107].

One can also attempt to quantitatively reconstruct the internal density distribution of the mantle for the relatively recent geological past during the evolution of the plate-mantle system. This reconstruction can be done by utilizing, or assimilating, geological information on past plate geometries and motions, for example by prescribing those kinematics, and then turning back the clock by reversing the flow in the mantle[108-113]. Such backward mantle convection methods are limited in their reliability to the last ~60 Ma and to those anomalies that are not advected into or out of thermal boundary layers and are subject to a range of uncertainties [109,114], but are possible because heat transport in vigorous thermal convection in the interior of the mantle is dominated by advection. However, diffusion becomes relevant over longer times, and in the thermal boundary layers, that is within the lithosphere and near the core mantle boundary. At the surface, paleo-age

grids can be used[115] as a constraint for past lithosphere thermal and density structure[110]. At depth, though, one must make other choices since diffusion is not time reversible.

However, such convection reconstructions can provide good first order estimates, for example of the time-evolving dynamic topography as associated with the transport of density anomalies toward the state at present as seen by seismic tomography [107,116-118].

[H2] Collision dynamics

On largest scales, the motion of Arabia is part of the closure of the Tethyan ocean which is at present reflected in broadly comparable patterns of collision and extrusion in the Anatolia-Arabia system in the west, and the India-South East Asia system in the East [52]. Within this system, previous models suggested that Arabia's northward movement relative to Africa is driven by the pull of the active subduction system in the Hellenic. The westward acceleration of the geodetic field supports this mechanism as the primary driving force [37,119].

The motion of Arabia has also been related to slab-pull [120,121]. However, there is evidence that the slab has been broken beneath the Bitlis suture, most likely since the middle Miocene [61,66,67,122], so that the only active subduction zone is confined to the Makran, where the subduction of oceanic lithosphere is still occurring [123]. This configuration, however, is likely too narrow to account for the motion of the entire Arabian plate. Another possible explanation is that the Afar plume is pushing Arabia northward, even though the constant velocity attained by Arabia during the last ~30 Ma [121] contrasts with the expected progressive decrease in velocity from a main upwelling plume phase at ~32 Ma [124]. Another possible model proposes that mantle drag related to a large-scale convection cell could efficiently pull continental plates toward collisional zones (Fig. 2), thus favoring indentation [37,78,125]. This conceptual model is supported by several arguments discussed in the following sections.

The development of a large-scale convection cell for mantle drag, however, requires the establishment of an efficient asthenospheric-scale circulation system involving both upwelling and downwelling. For such scenarios of links between the deep mantle and surface tectonics, seismic tomography anomalies can be helpful, either from direct interpretation, or from mantle circulation modeling, including going backward in time. While evidence of upwelling comes from the Afar Plume, the downwelling must be located beneath the collision zone.

One way to illustrate the links between tectonic evolution and tomography is by means of associating past subduction with convergent plate boundaries [92]. One such research effort is the "Atlas of the Underworld" [126] , which illustrates connections between a range of seismic tomography anomalies and tectonics, and their uncertainties. In the Tethys region, the Atlas identifies a number of separate slabs, associated with individual subduction zones that occurred in the collision zone.

For example, along the cross section shown in Figure 4, and conceptualized in the schematic Figure 2, ref. van der Meer, et al. [126] identify the Arabia at depth 1100-2200 km with top age 75-65 Ma, and the Mesopotamia slab at 1250-2200 km with top age 70-60 Ma ref. [126].

However, these two slabs are not clearly distinguishable in the tomography models, with exception for Model SEMUCB-WM1 (Supplementary Figure 5), which are the basis of the numerical model shown in Figure 4 and Supplementary Figures 1-5 and thus also of our schematic in Figure 2. The backward-advection procedure seeks to explore the convective paths over the last 10s of Myr of what has been imaged in tomography. This approach is most appropriate for mid-mantle structures and brings the tops of those regions of high seismic velocity, interpreted as high density at this depth range back close to the surface at 50 Ma. The results of this approach match well with the top ages of those slabs[126]. At that time, their bases are computed to be in the lower mantle. Hence, we estimate that those slabs entered the lower mantle somewhat earlier than 50 Ma. Further west, the entrance of the Aegean slab into the lower mantle has been estimated to have occurred at 50-40 Ma [37,127-129]. This slab can also be identified in the right-side upper part of the left most (top row) cross sections of Supplementary Figures 1-5.

Such backward-advection modeling indicates that the Aegean slab entered the lower mantle somewhat earlier than 50-40 Ma, related to its present-day extent somewhat deeper than 1400 km, according to the tomography models shown (Supplementary Figures 1-5). Further east below Iran and Afghanistan, ref. van der Meer, et al. [126] identified the Zagros and Sistan slabs. These slabs can also be identified in the cross sections of the tomography models displayed in Supplementary Figures 1-5: the Zagros slab can be seen – although somewhat smeared out - in the upper parts of the third-row, while the Sistan slab is in the middle parts of the fourth row. These global models do not distinguish so clearly between individual slabs and both horizontally and vertically, images are more like a continuous, although somewhat blobby, slab curtain.

Estimates of the age of tomographic anomalies critically depend on assumed or modeled slab sinking rate, and those are somewhat uncertain. For example, global correlation analysis based on mantle circulation modeling leads to sinking rates that are faster than those of ref. van der Meer, et al. [126] [130,131]. The entrance of the Tethyan slab into the lower mantle below Iran is less clear. However, there are two important episodes of regional upper plate subsidence that could have marked this event [49]. One occurred in the late Eocene and was associated with a widespread magmatic flare-up, while the other took place in the early Miocene and was linked to volcanism localized in proximity to the suture zone [132]. In terms of the establishment of a mantle convection cell, slabs do not need to reach the core-mantle boundary (CMB) to trigger plumes there. Rather, as soon as they have reached the high-viscosity lower mantle, they start pushing material ahead of them that could trigger plumes at the CMB. In regions of large-scale upwelling flow, the plume heads might take less than 30 Myr to reach the surface [133]. Hence slabs entering the lower mantle at ~60-50 Myr could have triggered the Afar plume reaching the surface at ~30 Ma.

In conclusion, the entrance of the slab into the lower mantle and Afar plume upwelling may be considered as connected, generating a convection cell, a conveyor belt, whose expression on the surface should be manifested by two main processes: topography and volcanism (Fig. 2). Whereas here we reconstruct past mantle structure by backward-advecting density anomalies inferred from tomography, an alternative approach uses subduction history to forward model mantle density and adjust the model to obtain a good fit with seismic tomography [134-136]. A slab sinking speed of 2 ± 0.8 cm/yr was determined by matching features that occur in both geodynamic and tomography models Steinberger, et al. [130], , a value substantiated by the analysis of ref. Peng and Liu [131]. Subducted slabs in such models will trigger plumes at the core-mantle boundary, particularly along margins of thermo-chemical piles [137-139] the locations of which can be compared to actual large igneous provinces [140]. Instead of imposing subduction zones, it is also possible to let them develop self-consistently. Also in this case, they will trigger plumes forming at the core-mantle boundary [141].

[H2] Plume arrival, mantle flow and volcanism

The development of the topography connecting Africa and Eurasia (the Middle East) began in the late Eocene. Around 40-35 million years ago (Ma), the Tethyan Ocean continued subducting beneath the Hellenic-Cyprus Arcs, while the Arabian continent moved toward the trench to the east, initiating an early incipient collision stage. Meanwhile, hundreds of kilometers south of this convergent margin, a large-scale uplift and doming process commenced (Fig. 3) in East Africa

(specifically the Ethiopian Plateau) and Yemen, gradually extending to northern Arabia (Fig. 1a) [11,30,31,33,142-145]. This uplift was likely linked to the arrival of the Afar plume and associated mantle flow, accompanied by volcanic activity that culminated in the massive eruption of the Ethiopian large igneous province around 35-30 Ma [27-29].

Beginning in the late Eocene and continuing through the Oligocene and early Miocene, volcanic activity, associated with mantle flow and subduction, deposited numerous volcanic rocks throughout the Tethys region and the region stretching from East Africa towards it (Fig. 3). This volcanic activity, related to mantle flow, appears to have migrated northward from present-day northeast Africa, eventually extending to northwest Arabia (Figs.1 & 3; [11,38,132]). By the early Miocene, the main zone of increased volcanism had reached what is northern Arabia, coinciding with the formation of the Gomphotherium land bridge and the closure of the Tethys Seaway (Fig. 3). Volcanic records, mantle flow models, and topographic reconstructions suggest a connection between mantle upwelling and surface uplift, which contributed to the formation of this land bridge

If the Afar plume arrived below the lithosphere around 35-30 million years ago (Ma) at approximately 8°N [146] and the land bridge occurred at ~20 Ma at ~30°N, this would imply a mantle flow speed of ~20 cm yr-1 – substantially faster than typical northward flow estimates of 5-10 cm yr-1 (for example, Fig 6. of ref. [147]; 10° of arrow length = 5 cm/yr). Mantle flow velocities could indeed be higher with lower asthenospheric viscosities, and northward flow may have been channeled between regions of thicker lithosphere, which are marked by faster seismic velocities in the uppermost mantle [37,38,148]. For example, assuming a channel width of 500 km, depth of 100 km, and density anomaly of 25 kg m-3 (equivalent to a temperature anomaly about 250 K), a mean flow speed of 20 cm yr-1 would correspond to a buoyancy flux of approximately $8 \cdot 10^3$ kg m-3. This buoyancy flux is notably higher than present-day estimates based on swell size, but buoyancy flux could have been much higher than today shortly after eruption of the plume head.

Similar flow speeds can also be estimated for other plumes. For example, in Iceland, radial viscous fingering of hot asthenosphere[149] (5 fingers, each 500 km wide and 100 km deep with 3% velocity anomaly corresponding to ~25 kg m-3 or 250 K; 28 Mg s-1 buoyancy flux) would result in an average flow speed of ~14 cm yr-1. However, 28 Mg s-1 is twenty times higher than an estimate based on swell size [150].

For the Canary plume, mantle plume material is thought to flow through a subcontinental lithospheric corridor beneath Africa to the Mediterranean[146]. With a channel width 250 km and

depth 100 km and the same density anomaly 25 kg m-3, a flow speed of 10 cm yr-1 (1500 km in 15 Myr) would correspond to a buoyancy flux of about 2 Mg s-1. This buoyancy flux is already twice the total plume flux estimated based on swell size [150], but tomography yields a much higher total plume flux estimate of about 10 Mg s-1 [151], in which case the flux through the corridor would be 20% of total plume flux. Part of such discrepancies might be caused by complicating effects of compositional buoyancy during fractionation, as well as the effects of nonlinear rheology which allows for local viscosity reduction and enhanced flow speeds compared to Newtonian approximations.

The Afar plume could have arrived beneath the lithosphere earlier, probably ~40 Ma[27], which would imply that the flow speeds necessary to align the timing and relative positions of the plume and the uplift could be lower than 20 cm yr-1. Based on several estimates [9,144], one can expect those dynamic topography contributions to be of kilometer-scale (Fig.4).

[H2] A land bridge supported by mantle flow

Backward circulation modeling can also help explore the role of time-variable convection on the topographic evolution of the Eastern Mediterranean [9]. Modelled mantle density anomalies capture the arrival of the Afar Plume and show the progression of a slow seismic and low density anomaly extending northward below Arabia (Fig.4). In Supplementary Figures 1-5 this can be seen in the second-row cross sections, but not the other cross sections to the left and right, consistent with the concept of a columnar plume upwelling that feeds into a sublithospheric channel towards the north. Comparison between geodynamic estimates based on different tomography models, a crude measure of "uncertainty", shows that this convective scenario is a robust result found from most tomographic models. This geometry contrasts with the subducted slabs, which are also consistently imaged, but with subduction occurring on a broad front, although a careful analysis of high-resolution tomography [126] can identify separate individual slabs as part of this front. The surface expression of this northward progression can be seen from the timing and composition of regional volcanic centers [36-38,132] (Fig.3).

Mantle dynamics in the region thus seems associated with a convection cell where the deep upwelling beneath the Horn of Africa is connected to a downwelling in the Tethyan region, forming a whole mantle convection cell, or a "conveyor belt" (Fig. 2) [37,78]. The Afar plume could be dragged

by mantle flow and advance in the upper mantle below the plate at a velocity that is faster than the surface speed of the plate due to Poiseuille (pressure driven) flow effects in the lower viscosity asthenosphere, as shown in the numerical models of ref. [9]. Such regional "mantle leading the plate" flow agrees well with the northward progression of volcanism [36,38], and the positive dynamic topography anomaly likewise migrates northward, supporting prior numerical models [89,106,107,118,152,153]. The time-dependent convective scenario of Fig. 4 shows how mantle convection could have influenced the topographic evolution of Arabia. Mantle flow from the Afar plume causes northwardly progressing uplift and volcanism, which had a role in the seaway closure and the formation of the Arabian-Eurasian land bridge. A regional-scale geodynamic model based on tomography supports this finding, showing the presence of mantle flow from the Arabian Plateau towards the East Anatolian Plateau[10]

The mantle flow and associated volcanism likely controlled the nature and timing of the Tethys Seaway final closure and the establishment of the land bridge. While the deep oceanic part of the gateway closed due to plate tectonic subduction, convergence and collision, the Mesopotamian Trough remained open until the Miocene (20 -19 Ma) when the plume material advected by northward mantle flow reached today's Middle East causing uplift. Regional volcanism [38,132] and paleogeographic reconstructions [9] show that mantle flow induced volcanism and uplift reached the location of the seaway in the early Miocene (Figs. 3 & 6), which likely impacted the topography, closed the Mesopotamian Through, and caused the land bridge to emerge much earlier than it would have without the plume influence (Figs. 3 & 4).

The interplay between deep mantle flow and surface processes highlights how internal Earth processes can control the surface morphology in the Tethys region. The next sections explore how these tectonic and geodynamic processes induced ocean circulation, climate, biogeographic changes by closing the Neothethys and controlling the formation the *Gomphoterium* land bridge.

[H1] Implications of land bridge formation

Paleogeographic changes in the Tethyan region influenced ocean circulation and climate far beyond the Mediterranean-Tethyan realm and resulted in massive faunal migrations between Africa Eurasia peaking in the Middle Miocene. Here we examine the consequences of seaway closure and land bridge formation, which likely had an important role in developing the modern ocean circulation and climate system, as well as influencing faunal migrations and likely also human evolution.

[H2] Consequences for marine circulation

The isolation of the eastern and western parts of the Neotethys had major consequences in the marine domain and occurred in two steps: first with the closure of the Neotethys deep oceanic gateway between 40 and 30 Ma [9], following the complete disappearance of the Neotethyan slab through subduction in the collision zone. Second, with the drying of the shallow Mesopotamian Trough, occurring first in the early Miocene (20-19 Ma), re-flooded in the early middle Miocene, but fully achieved by the middle Miocene (~ 14 Ma) [9,72-74]. The long-term fall of the sea level since the late Eocene, in response to reduced mid-oceanic-spreading and the growth of the polar ice caps [154,155] likely contributed to the retreat and later closure of the Mesopotamian Trough. Temporary re-flooding(s) of the seaway (~ 16 Ma - 14 Ma) could have been triggered by averagely higher mid-Miocene eustatic levels [156], and the final closure of the Mesopotamian Trough coincided with the sea level drop caused by Antarctica ice-sheet expansion at ca. 13.8 Ma [72]. However, the paleobathymetric changes required to close the seaway from depths of > 500 m in the middle Oligocene to subaerial in the middle Miocene [9,157] (Figure 3) are much greater than the most extreme paleo-sea level changes proposed during that period (with maximum of ~ 120 m) [158-160]. Topographic changes related post-collisional tectonics and/or mantle plume dynamics are thus needed to explain the evolution of the Mesopotamian Trough [9].

The main consequence of this protracted closure is a gradual and irreversible decrease in water throughflow resulting in an overall increase in sea surface salinity and water temperatures in the western Neotethys. Several climate sensitivity experiments closing Neotethyan and Paratethyan connections with the Atlantic also promote higher salinities in the North Atlantic [161-163]. This high salinity is an important condition for deep water formation in the North Atlantic and a critical step for the onset of the Atlantic Meridional Overturning Circulation (AMOC) [164,165].

The impact of the first closure step of the Neotethyan seaway on the proto-AMOC during the Eocene and Early Oligocene remains yet to be clearly drawn (Figure 5). Coupled global earth system model experiments of Straume, et al. [163] show that shallowing the seaway in the Late Eocene to 150 m, while keeping it relatively wide (~ 500 km), increase the surface salinity of the North Atlantic (by > 5 psu) and triggers a spike in North Atlantic Deep Water (NADW) formation and the proto-AMOC (to ~ 10 Sv). However, the increase in overturning disappears when their simulation stabilizes. Fully closing the seaway with Eocene boundary conditions, as in Zhang, et al. [161], triggers a more permanent increase in the NADW and the proto-AMOC (to ~12 Sv). Closing

other nearby seaways, such as the Danish-Polish Trough (the proto-Paratethys - North Sea connection further North), show a similar effect on Eocene sea surface salinities [162], but whether this triggers a proto-AMOC depends on the configuration of the Atlantic – Arctic oceanic gateways. It is thus difficult to quantitatively assess the impact of the sole protracted Neotethyan oceanic gateway closure on the proto-AMOC as it depends on several factors such as nearby oceanic gateways (e.g. the Atlantic – Arctic gateways and Polish Trough), the global paleogeography, and background climate state [161-164,166].

Isotopic tracers for marine currents indicate indicates the persistence of a significant water throughflow even after the disappearance of the deep oceanic gateway, until the second step of Neotethyan closure associated with the drying of the Mesopotamian Trough in the early Miocene [72]. However, the impact of this second closure step on the AMOC and global oceanic circulation is also controversial. The climate sensitivity study by Hamon, et al. [167] shows that the closure of the Mesopotamian Trough strengthens the AMOC (by 3-6 Sv) and the Tethyan Indian Saline Water (TISW, discussed below) when the seaway depth go from a 1000 m to 250 m, while Pillot, et al. [166] find little impact on the North Atlantic surface salinity and AMOC when the seaway depth changes from 120 m to closed. Recent paleogeographic reconstructions show that the latter is likely more realistic for the Mid Miocene, as the Mesopotamian Trough was very shallow [9,157], while the effects modelled by Hamon, et al. [167] are more relevant for the shoaling from late Oligocene to the early Miocene.

The ocean circulation changes from the closure of the Neotethys Mesopotamian Trough in the Miocene are also not fully understood. When the seaway is open, most modelling studies show a surface flow oriented from the Indo-Pacific towards the Mediterranean and Atlantic Ocean [161,163,164,168](Figure 5). However, there may have been a flow of intermediate and deep saline waters flowing in the other direction, towards the Indian Ocean [167,169,170]. This eastward flow could have induced a warm and saline water mass in the Indian Ocean [167] corresponding to the TISW[169]. The closure of the Neotethys could then have freshened and cooled the Indian Ocean [167,170], impacting the latitudinal density gradient and resulting in an intensification of the Antarctic Circumpolar Current [167]. More recently, the climate modeling study of Sarr, et al. [171] suggest that the final closure of the Mesopotamian Trough triggered the emplacement of marine upwelling along the Arabian coast, favoring marine productivity blooms and setting up the modern large-scale oceanic circulation in the Indian Ocean.

There is thus no clear consensus among climate modeling studies on the relative impact of the disappearance of the deep oceanic gateway versus the later drying of the Mesopotamian Trough on the AMOC and establishment of the modern-day global ocean circulation [161,167]. The closure of the Neotethys has to be considered in combination with other paleogeographic changes surrounding the Atlantic, including variations in the Atlantic – Arctic Oceanic gateways [163-165,172], closure of the Central American Seaway [173,174], and the opening of the Southern Ocean gateways [175-178], and future ocean and climate modelling studies should include a realistic two-step closure model to determine the relative role of the Neotethys through time. However, based on previous climate simulations, it does seem that the closure of the Neotethys was a necessary domino to fall for the transition from a global circulation mode dominated by Southern Ocean Deep Water to one dominated by North Atlantic Deep Water [161].

[H2] Consequences for the oceanic Carbon cycle

The closure of the Neotethys had also an indirect impact on the oceanic carbon cycle. Following the onset of the soft collision stage, crustal shortening and thickening resulted in the gradual emergence of the Anatolian and Iranian segments of the Eurasian Neotethyan subduction zone [39,179,180]. This emergence caused the drying of the last latitudinal seaways connecting the Neotethys and Paratethys, in times as early as the middle-late Eocene (~45 Ma – 35 Ma; Fig. 5), around the time when atmospheric CO_2 dropped from ~1000 ppm to ~500 ppm [181] (Figure 6). The increased isolation of Paratethys waters resulted in the development of widespread anoxic conditions starting episodically in the late middle Eocene and fully achieved in the earliest Oligocene [182]. These changes in the global oceanic circulation have been proposed to enhance organic carbon sequestration and favor the late Paleogene global cooling trend [68], by reducing atmospheric pCO_2, although no quantification has been published yet. Exhumation, river integration, and sediment transport associated with the closure and subsequent mantle plume dynamics could also have played a minor role in the late Paleogene CO_2 drop. Their impact has not been modeled nor fully quantified yet. Exhumation rates significantly increased during the middle-late Eocene onwards from central Anatolia to Iran [183] (Figure 6), where easily weatherable, mafic and ultramafic rocks are widespread. Further south, the integration of the Nile River drainage, possibly starting as early as the Oligocene in response to nascent uplift in eastern Africa, was associated with the erosion of rather mature basement rocks [184]. However, the paleo-position of these two areas during the late Paleogene, outside the tropical domain, suggests a poor weatherability of the whole region [185]. Sediment fluxes from the Nile River start to have a noticeable impact only much later, during the middle-late Miocene. Since then, their variations drive

ocean productivity and water stratification in the eastern Mediterranean, resulting in the deposition of organic-rich sapropels with an extraordinary orbital regularity [186].

[H2] A contrasted hydroclimate response on land

Climate sensitivity modeling studies show that the gradual emergence and uplift associated with the Neotethyan closure have dramatic and different impacts on the hydroclimate of both the African and Eurasian sides of the collision zone. The emergence of the Arabian Peninsula locally altered sea-surface temperatures in nearby oceanic basins and resulted in strengthened seasonal temperature gradients and increased regional aridity in a wide belt from north Africa to central Asia [187,188]. It notably reduced northeastwards heat transport from the Atlantic into Africa and dampened the African monsoon [189]. This process is already observed in Oligocene climate simulations [187], and likely reached its climax during the Miocene. This aridity trend was likely enhanced by Miocene uplift in eastern Africa related to mantle plume dynamics, which further reduced the northeastward penetration of African monsoonal moisture [190]. The chronology of eastern Africa uplift remains poorly documented, and it is unclear when this effect started to kick in. The final drying of the Mesopotamian Trough has been proposed as a final trigger for Saharan desertification in the late middle Miocene [189]. This event predates the age of the oldest dated Saharan dunes ca. 7 Ma [191] (Figure 6).

By contrast, the same emergence and topographic uplift enhanced the Somali jet offshore the Arabian coast and increased monsoonal moisture transport inland South Asia [171]. The onset of high productivity offshore the Arabian coast, which is commonly associated with a strong Somali Jet, appears synchronous with the last drying of the Mesopotamian Trough [171,192]. The later (Mio-Pliocene) uplift of the Zagros, Iranian Plateau and Anatolian Plateau [56] reduced the penetration of westerlies into South Asia, further enhancing monsoonal transport via the Gangetic Jet in India and Pakistan [12,193]. Overall, the topographic changes associated with the plume migration enhanced Asian monsoonal rainfall and wettened South Asia.

[H2] The end of Island Africa

The formation of the *Gomphotherium* land bridge ended 75 Myr of African biogeographic isolation [194]. Cretaceous and Paleogene terrestrial fauna of Africa were highly endemic, poorly diversified and renewed by discrete pulses of sweepstake dispersal from Laurasia. But in the early Miocene, the creation of the *Gomphotherium* land bridge generated a wave of massive dispersal known as

the Great Old World Biotic Interchange (GOWBI) [14]. The GOWBI, like the earlier *Grande Coupure* [180] and later GABI (Great American Biotic Interchange) [195], is a classic example of large-scale geodispersal and highlights the fate of endemic taxa when they are put into contact with a wider, more diverse population.

As seen for the *Grande Coupure* and the GABI, mammalian exchanges between the two continental masses were asymmetric: most of the species involved in the geodispersal were Asian taxa reaching Africa, including rodents (members of muridae, scuiridae, spalacidae families), artiodactyls (bovidae, anthracotheriidae, giraffidae, suidae), carnivora (mustelidae, ursidae, felidae, viverridae), and perissodactyls (rhinocerotidae, chalicotheriidae) [14]. Their arrival into Africa resulted in the extinction of multiple endemic clades, such as embrithopods, many hyracoids and other afrotherian mammals, as well as several lineages of endemic rodents. Nonetheless, several African endemic taxa successfully made it to Asia, including hyaenodonts and multiple species of proboscideans (and the iconic *Gomphotherium*) [196].

The perhaps most interesting dispersal event related to the closure of the Neotethys involves crown anthropoid primates. The first anthropoid primates are known from Asia in the middle Eocene, and they are one of the few clades that dispersed to Africa before the GOWBI during the late middle Eocene [15]. This dispersal might have been favored by the incipient closure of the Neotethys and the use of Balkanatolian islands as steppingstones [180,197]. While anthropoid primates got extinct in Asia during the Oligocene, their African lineages diversified on Island Africa [198], and re-colonized Asia during the GOWBI[14].

The magnitude of the GOWBI, both in the distance covered by some taxa and the amount of involved species, is particularly surprising considering that the emergence of the peninsula promoted aridification and must have reduced and partitioned arboreal habitats at continental scale [189]. The presence of a wide desert over the Middle East, as predicted by some climate models [12], should have significantly limited biotic interchanges. Paleoenvironmental data on the dispersal pathway are unfortunately scarce before the late Miocene [199]. Early Miocene Eastern African ecosystems displayed a high heterogeneity with forested and grassland habitats, hosting some of the first C4 plants [200]. In Central Asia, early Miocene ecosystems were dominated by steppe-desert taxa, where grasses only played a minor role [201]. South Asia has yielded multiple early Miocene fossil wood taxa indicating the presence of seasonally wet, monsoonal tropical forests [202]. The ecosystems of the buffer zone between these three areas, across the Arabian Peninsula, the Levant,

and modern Iran, remain virtually undocumented for the early Miocene. This paradox remains to be explained by further data, as well as with ecological niche modeling studies associated with detailed paleogeographic reconstructions.

The gradual isolation of the western Neotethys from the soon-to-be Indian Ocean also led to the development of the endemic Mediterranean aquatic fauna. Fossil taxa and molecular clocks date back the divergence of several western Neotethyan marine clades up to the late middle Eocene, such as for killifishes or estuarine gastropods [203,204]. Most western Neotethyan taxa yield divergence estimates around the Oligocene and early Miocene times, indicating that the creation of the *Gomphotherium* landbridge irreversibly isolated Mediterranean aquatic taxa [70,205]. This isolation is associated with a shift of marine biodiversity from the western Neotethys to the Indo-West Pacific, and only few species including echinoderms; [70], dispersed between both biogeographic provinces during the ephemeral middle Miocene re-opening of the Mesopotamian Trough.

In Summary, the two-step closure of the Neotethys created cascading effects on oceanic heat and salinity distribution, regional aridification and monsoon patterns, and faunal dispersal routes. These interconnected changes underscore the role of tectonic and deep Earth processes in driving Earth's climatic transitions and shaping biodiversity over geologic timescales.

[H1] Summary and future perspectives

The geology of the Eastern Mediterranean region has recorded complex interactions between subduction, continental collision, mantle dynamics, and topography. The deeper parts of the Tethys Seaway closed due to tectonic convergence and collision, but ultimately the shallower portions closed with the formation of the *Gomphotherium* land bridge due to mantle convection and volcanism. Based on the age of the Ethiopian flood basalts [29] it is estimated that the Afar Plume arrived below the lithosphere in the early Oligocene, at ~ 31 Ma, then further north reaching Sinai northwest Arabia by ~20 Ma in the early Miocene, which correlates with volcanic activity trending younger towards the north. Mantle flow generated kilometer scale uplift from East Africa, at ~8°N at ~31 Ma [146], along Arabia, and generated the *Gomphotherium* landbridge at 30°N ~20 Ma. The emergence of the land bridge marks the end of the marine gateway between the Atlantic, proto-Mediterranean, and Indo-Pacific Oceans, which impacted marine and terrestrial diversification and migration patterns, as well as ocean circulation and climate.

In the classical "Wilson type" [206] plate tectonic scenario, the arrival of a continental block in a subduction zone causes the onset of large-scale crustal thickening and shutdown of subduction. When viewed with a mantle convection context, however, the push of the continental block could be sustained if driven by large-scale convection cells including active mantle upwellings and slab pull from the downgoing attached oceanic part of the plate e.g., [207] (Fig. 2). Ultimately, the collisional processes leading to extreme crustal thickening, such as the one observed along the Tethyan realm in the Himalaya-Tibet or in the Turkish-Iranian plateau, could only occur under the protracted and vigorous action of mantle convection. The time-dependent signatures of this process on the surface included volcanism and dynamic topography [9,38,132]. Generating large-scale mountain belts through the collision of continents following subduction represents a specific mechanism and it requires prolonged kinematic convergence leading to an increase in gravitational potential energy. Drivers for this mechanism require either a distinctive tectonic organization or contributions from the mantle. Such reorganizations could, however, have happened several times during the coevolution of continental dynamics and mantle convection, and hence represent a generally relevant process. The efforts to fully understand such processes, and in particular how they are expressed in the geological record, including their consequences on the topography evolution and on ocean circulation, climate, and biogeography, are still in their infancy stages.

While substantial progress has been made, mantle dynamics and tectonics in the Mediterranean-Tethyan region remain a complex puzzle, and there are several critical aspects that need further exploration. For example, the role of the Afar Plume could be important not only for generating regional uplift, but also for affecting plate motions by means of modifying the asthenospheric viscosity. A better understanding of the dynamics in the region should be the subject of future research efforts. For example, by studying the interaction of the Afar plume with large-scale mantle flow and a lithosphere of variable thickness. This interaction could be both ways in that plume material is being channeled towards regions of already thinned lithosphere in the direction where it is pushed by the mantle wind, but in these regions also further erodes and thins the lithosphere from underneath.

Furthermore, more geological data constraining the uplift history of the collisional system and the environmental changes associated with the formation of the *Gomphotherium* landbridge are needed to better constrain the surface and atmospheric expression of these dynamics. Where, for example, more detailed special and temporal uplift models should be incorporated in the paleogeography of paleoclimate models to more realistically simulate consequences for regional and global ocean circulation and climate.

An important aspect of future work should be the exploration of the relative role of paleogeography and climatic changes on the biogeographic dispersal of terrestrial species, which has become more accessible with paleoclimate simulations [161,163,167,171,187] and realistic paleogeographic reconstructions [9,208-211]. Dispersal occurrences not only depend on available pathways provided by paleogeography, but also the environment and climatic conditions.

[H1] References

1 Jolivet, L. & Faccenna, C. Mediterranean extension and the Africa-Eurasia collision. *Tectonics* **19**, 1095-1106, doi:10.1029/2000tc900018 (2000).

2 Stampfli, G. Plate tectonics of the Apulia-Adria microcontinents. *CROP Project-Deep Seismic explorations of the Central Mediterranean and Italy, Section* **11**, 747-766 (2005).

3 Mouthereau, F. Timing of uplift in the Zagros belt/Iranian plateau and accommodation of late Cenozoic Arabia–Eurasia convergence. *Geological Magazine* **148**, 726-738, doi:10.1017/S0016756811000306 (2011).

4 Cavazza, W., Albino, I., Galoyan, G., Zattin, M. & Cattò, S. Continental accretion and incremental deformation in the thermochronologic evolution of the Lesser Caucasus. *Geoscience Frontiers* **10**, 2189-2202, doi:https://doi.org/10.1016/j.gsf.2019.02.007 (2019).

5 Dercourt, J. *et al.* Geological evolution of the tethys belt from the atlantic to the pamirs since the LIAS. *Tectonophysics* **123**, 241-315, doi:https://doi.org/10.1016/0040-1951(86)90199-X (1986).

6 Gaina, C., Hinsbergen, D. J. & Spakman, W. Tectonic interactions between India and Arabia since the Jurassic reconstructed from marine geophysics, ophiolite geology, and seismic tomography. *Tectonics* **34**, 875-906 (2015).

7 Gaina, C. *et al.* The African Plate: A history of oceanic crust accretion and subduction since the Jurassic. *Tectonophysics* **604**, 4-25 (2013).

8 Torsvik, T. H., Smethurst, M. A., Burke, K. & Steinberger, B. Large igneous provinces generated from the margins of the large low-velocity provinces in the deep mantle. *Geophysical Journal International* **167**, 1447-1460 (2006).

9 Straume, E. O., Steinberger, B., Becker, T. W. & Faccenna, C. Impact of mantle convection and dynamic topography on the Cenozoic paleogeography of Central Eurasia and the West Siberian Seaway. *Earth and Planetary Science Letters* **630**, 118615, doi:https://doi.org/10.1016/j.epsl.2024.118615 (2024).

10 Şengül Uluocak, E., Pysklywec, R. N., Sembroni, A., Brune, S. & Faccenna, C. The Role of Upper Mantle Forces in Post-Subduction Tectonics: Plumelet and Active Rifting in the East Anatolian Plateau. *Geochemistry, Geophysics, Geosystems* **25**, e2024GC011639, doi:https://doi.org/10.1029/2024GC011639 (2024).

11 Sembroni, A., Faccenna, C., Becker, T. W. & Molin, P. The uplift of the East Africa - Arabia swell. *Earth-Science Reviews* **257**, 104901, doi:https://doi.org/10.1016/j.earscirev.2024.104901 (2024).

12 Tardif, D. *et al.* The role of paleogeography in Asian monsoon evolution: a review and new insights from climate modelling. *Earth-Science Reviews* **243**, 104464, doi:https://doi.org/10.1016/j.earscirev.2023.104464 (2023).

13 van Hinsbergen, D. J. J. *et al.* Orogenic architecture of the Mediterranean region and kinematic reconstruction of its tectonic evolution since the Triassic. *Gondwana Research* **81**, 79-229, doi:https://doi.org/10.1016/j.gr.2019.07.009 (2020).

14 Rage, J.-C. & Gheerbrant, E. in *Biological Consequences of Plate Tectonics: New Perspectives on Post-Gondwana Break-up–A Tribute to Ashok Sahni* (eds Guntupalli V. R. Prasad & Rajeev Patnaik) 251-264 (Springer International Publishing, 2020).

15 Chaimanee, Y. *et al.* Early anthropoid primates: New data and new questions. *Evolutionary Anthropology: Issues, News, and Reviews* **n/a**, e22022, doi:https://doi.org/10.1002/evan.22022 (2024).

16 Leroy, S. *et al.* 385-427 (Springer Berlin Heidelberg).

17 Augustin, N., van der Zwan, F. M., Devey, C. W. & Brandsdóttir, B. 13 million years of seafloor spreading throughout the Red Sea Basin. *Nature Communications* **12**, 2427, doi:10.1038/s41467-021-22586-2 (2021).

18 ArRajehi, A. *et al.* Geodetic constraints on present-day motion of the Arabian Plate: Implications for Red Sea and Gulf of Aden rifting. *Tectonics* **29**, doi:https://doi.org/10.1029/2009TC002482 (2010).

19 Ghebreab, W. Tectonics of the Red Sea region reassessed. *Earth-Science Reviews* **45**, 1-44 (1998).

20 Bosworth, W., Huchon, P. & McClay, K. The Red Sea and Gulf of Aden Basins. *Journal of African Earth Sciences* **43**, 334-378, doi:https://doi.org/10.1016/j.jafrearsci.2005.07.020 (2005).

21 Nuriel, P., Weinberger, R., Kylander-Clark, A. R. C., Hacker, B. R. & Craddock, J. P. The onset of the Dead Sea transform based on calcite age-strain analyses. *Geology* **45**, 587-590, doi:10.1130/g38903.1 (2017).

22 Fournier, M. *et al.* Owen Fracture Zone: The Arabia–India plate boundary unveiled. *Earth and Planetary Science Letters* **302**, 247-252, doi:https://doi.org/10.1016/j.epsl.2010.12.027 (2011).

23 Bayer, H. J., Hötzl, H., Jado, A. R., Röscher, B. & Voggenreiter, W. Sedimentary and structural evolution of the northwest Arabian Red Sea margin. *Tectonophysics* **153**, 137-151, doi:https://doi.org/10.1016/0040-1951(88)90011-X (1988).

24 Pik, R. *et al.* Structural control of basement denudation during rifting revealed by low-temperature (U–Th–Sm)/He thermochronology of the Socotra Island basement—Southern Gulf of Aden margin. *Tectonophysics* **607**, 17-31, doi:https://doi.org/10.1016/j.tecto.2013.07.038 (2013).

25 Purcell, P. G. Re-imagining and re-imaging the development of the East African Rift. *Petroleum Geoscience* **24**, 21-40, doi:https://doi.org/10.1144/petgeo2017-036 (2018).

26 Boone, S. C., Balestrieri, M.-L. & Kohn, B. Tectono-Thermal Evolution of the Red Sea Rift. *Frontiers in Earth Science* **9**, doi:10.3389/feart.2021.713448 (2021).

27 Ebinger, C. J. & Sleep, N. H. Cenozoic magmatism throughout east Africa resulting from impact of a single plume. *Nature* **395**, 788-791, doi:10.1038/27417 (1998).

28 Rooney, T. O. The Cenozoic magmatism of East-Africa: Part I — Flood basalts and pulsed magmatism. *Lithos* **286-287**, 264-301, doi:https://doi.org/10.1016/j.lithos.2017.05.014 (2017).

29 Hofmann, C. *et al.* Timing of the Ethiopian flood basalt event and implications for plume birth and global change. *Nature* **389**, 838-841, doi:10.1038/39853 (1997).

30 Şengör, A. C. Elevation as indicator of mantle-plume activity. *Mantle plumes: their identification through time. Geological Society of America Special Paper* **352**, 183-225 (2001).

31 Avni, Y., Segev, A. & Ginat, H. Oligocene regional denudation of the northern Afar dome: Pre- and syn-breakup stages of the Afro-Arabian plate. *GSA Bulletin* **124**, 1871-1897, doi:10.1130/b30634.1 (2012).

32 Sembroni, A., Faccenna, C., Becker, T. W., Molin, P. & Abebe, B. Long-term, deep-mantle support of the Ethiopia-Yemen Plateau. *Tectonics* **35**, 469-488, doi:https://doi.org/10.1002/2015TC004000 (2016).

33 Bar, O., Zilberman, E., Feinstein, S., Calvo, R. & Gvirtzman, Z. The uplift history of the Arabian Plateau as inferred from geomorphologic analysis of its northwestern edge. *Tectonophysics* **671**, 9-23, doi:https://doi.org/10.1016/j.tecto.2016.01.004 (2016).

34 Krienitz, M.-S., Haase, K. M., Mezger, K. & Shaikh-Mashail, M. A. Magma Genesis and Mantle Dynamics at the Harrat Ash Shamah Volcanic Field (Southern Syria). *Journal of Petrology* **48**, 1513-1542, doi:10.1093/petrology/egm028 (2007).

35 Krienitz, M.-S. *et al.* Tectonic events, continental intraplate volcanism, and mantle plume activity in northern Arabia: Constraints from geochemistry and Ar-Ar dating of Syrian lavas. *Geochemistry, Geophysics, Geosystems* **10**, doi:https://doi.org/10.1029/2008GC002254 (2009).

36 Ershov, A. & Nikishin, A. Recent geodynamics of the Caucasus-Arabia-east Africa region. *Geotectonics* **38**, 123-136 (2004).

37 Faccenna, C., Becker, T. W., Jolivet, L. & Keskin, M. Mantle convection in the Middle East: Reconciling Afar upwelling, Arabia indentation and Aegean trench rollback. *Earth and Planetary Science Letters* **375**, 254-269, doi:https://doi.org/10.1016/j.epsl.2013.05.043 (2013).

38 Hua, J., Fischer, K. M., Gazel, E., Parmentier, E. M. & Hirth, G. Long-Distance Asthenospheric Transport of Plume-Influenced Mantle From Afar to Anatolia. *Geochemistry, Geophysics, Geosystems* **24**, e2022GC010605, doi:https://doi.org/10.1029/2022GC010605 (2023).

39 Ballato, P. *et al.* Arabia-Eurasia continental collision: Insights from late Tertiary foreland-basin evolution in the Alborz Mountains, northern Iran. *GSA Bulletin* **123**, 106-131, doi:10.1130/b30091.1 (2011).

40 Agard, P. *et al.* Zagros orogeny: a subduction-dominated process. *Geological Magazine* **148**, 692-725, doi:10.1017/S001675681100046X (2011).

41 Tadayon, M. *et al.* The long-term evolution of the Doruneh Fault region (Central Iran): A key to understanding the spatio-temporal tectonic evolution in the hinterland of the Zagros convergence zone. *Geological Journal* **54**, 1454-1479, doi:https://doi.org/10.1002/gj.3241 (2019).

42 Barber, D. E., Stockli, D. F., Horton, B. K. & Koshnaw, R. I. Cenozoic Exhumation and Foreland Basin Evolution of the Zagros Orogen During the Arabia-Eurasia Collision, Western Iran. *Tectonics* **37**, 4396-4420, doi:https://doi.org/10.1029/2018TC005328 (2018).

43 Darin, M. H. & Umhoefer, P. J. Diachronous initiation of Arabia–Eurasia collision from eastern Anatolia to the southeastern Zagros Mountains since middle Eocene time. *International Geology Review* **64**, 2653-2681, doi:10.1080/00206814.2022.2048272 (2022).

44 Berberian, F. & Berberian, M. in *Zagros Hindu Kush Himalaya Geodynamic Evolution* 5-32 (1981).

45 Okay, A. I., Zattin, M. & Cavazza, W. Apatite fission-track data for the Miocene Arabia-Eurasia collision. *Geology* **38**, 35-38, doi:10.1130/g30234.1 (2010).

46 McQuarrie, N. & van Hinsbergen, D. J. J. Retrodeforming the Arabia-Eurasia collision zone: Age of collision versus magnitude of continental subduction. *Geology* **41**, 315-318, doi:10.1130/g33591.1 (2013).

47 Pirouz, M., Avouac, J.-P., Hassanzadeh, J., Kirschvink, J. L. & Bahroudi, A. Early Neogene foreland of the Zagros, implications for the initial closure of the Neo-Tethys and kinematics of crustal shortening. *Earth and Planetary Science Letters* **477**, 168-182, doi:https://doi.org/10.1016/j.epsl.2017.07.046 (2017).

48 Koshnaw, R. I., Stockli, D. F. & Schlunegger, F. Timing of the Arabia-Eurasia continental collision—Evidence from detrital zircon U-Pb geochronology of the Red Bed Series strata of the northwest Zagros hinterland, Kurdistan region of Iraq. *Geology* **47**, 47-50, doi:10.1130/g45499.1 (2018).

49 Boutoux, A. *et al.* Slab Folding and Surface Deformation of the Iran Mobile Belt. *Tectonics* **40**, e2020TC006300, doi:https://doi.org/10.1029/2020TC006300 (2021).

50 Cavazza, W., Cattò, S., Zattin, M., Okay, A. I. & Reiners, P. Thermochronology of the Miocene Arabia-Eurasia collision zone of southeastern Turkey. *Geosphere* **14**, 2277-2293, doi:10.1130/ges01637.1 (2018).

51 Paul, A., Kaviani, A., Hatzfeld, D., Vergne, J. & Mokhtari, M. Seismological evidence for crustal-scale thrusting in the Zagros mountain belt (Iran). *Geophysical Journal International* **166**, 227-237, doi:10.1111/j.1365-246X.2006.02920.x (2006).

52 Hatzfeld, D. & Molnar, P. Comparisons of the kinematics and deep structures of the Zagros and Himalaya and of the Iranian and Tibetan plateaus and geodynamic implications. *Reviews of Geophysics* **48**, doi:https://doi.org/10.1029/2009RG000304 (2010).

53 Cavazza, W. *et al.* Two-step exhumation of Caucasian intraplate rifts: A proxy of sequential plate-margin collisional orogenies. *Geoscience Frontiers* **15**, 101737, doi:https://doi.org/10.1016/j.gsf.2023.101737 (2024).

54 Zanchi, A., Berra, F., Mattei, M., R. Ghassemi, M. & Sabouri, J. Inversion tectonics in central Alborz, Iran. *Journal of Structural Geology* **28**, 2023-2037, doi:https://doi.org/10.1016/j.jsg.2006.06.020 (2006).

55 Robert, A. M. M. *et al.* Structural evolution of the Kopeh Dagh fold-and-thrust belt (NE Iran) and interactions with the South Caspian Sea Basin and Amu Darya Basin. *Marine and Petroleum Geology* **57**, 68-87, doi:https://doi.org/10.1016/j.marpetgeo.2014.05.002 (2014).

56 Molin, P., Sembroni, A., Ballato, P. & Faccenna, C. The Uplift of an Early Stage Collisional Plateau Unraveled by Fluvial Network Analysis and River Longitudinal Profile Inversion: The Case of the Eastern Anatolian Plateau. *Tectonics* **42**, e2022TC007737, doi:https://doi.org/10.1029/2022TC007737 (2023).

57 Cowgill, E. *et al.* Relict basin closure and crustal shortening budgets during continental collision: An example from Caucasus sediment provenance. *Tectonics* **35**, 2918-2947, doi:https://doi.org/10.1002/2016TC004295 (2016).

58 Jackson, J., Priestley, K., Allen, M. & Berberian, M. Active tectonics of the South Caspian Basin. *Geophysical Journal International* **148**, 214-245, doi:10.1046/j.1365-246X.2002.01588.x (2002).

59 Cifelli, F., Ballato, P., Alimohammadian, H., Sabouri, J. & Mattei, M. Tectonic magnetic lineation and oroclinal bending of the Alborz range: Implications on the Iran-Southern Caspian geodynamics. *Tectonics* **34**, 116-132, doi:https://doi.org/10.1002/2014TC003626 (2015).

60 Gürer, D. & van Hinsbergen, D. J. J. Diachronous demise of the Neotethys Ocean as a driver for non-cylindrical orogenesis in Anatolia. *Tectonophysics* **760**, 95-106, doi:https://doi.org/10.1016/j.tecto.2018.06.005 (2019).

61 Faccenna, C., Bellier, O., Martinod, J., Piromallo, C. & Regard, V. Slab detachment beneath eastern Anatolia: A possible cause for the formation of the North Anatolian fault. *Earth and Planetary Science Letters* **242**, 85-97, doi:https://doi.org/10.1016/j.epsl.2005.11.046 (2006).

62 Şengör, A. M. C. *et al.* THE NORTH ANATOLIAN FAULT: A NEW LOOK. *Annual Review of Earth and Planetary Sciences* **33**, 37-112, doi:https://doi.org/10.1146/annurev.earth.32.101802.120415 (2005).

63 Racano, S., Schildgen, T., Ballato, P., Yıldırım, C. & Wittmann, H. Rock-uplift history of the Central Pontides from river-profile inversions and implications for development of the North Anatolian Fault. *Earth and Planetary Science Letters* **616**, 118231, doi:https://doi.org/10.1016/j.epsl.2023.118231 (2023).

64 Jolivet, L. *et al.* Aegean tectonics: Strain localisation, slab tearing and trench retreat. *Tectonophysics* **597-598**, 1-33, doi:https://doi.org/10.1016/j.tecto.2012.06.011 (2013).

65 Kounoudis, R. *et al.* Seismic Tomographic Imaging of the Eastern Mediterranean Mantle: Implications for Terminal-Stage Subduction, the Uplift of Anatolia, and the Development of the North Anatolian Fault. *Geochemistry, Geophysics, Geosystems* **21**, e2020GC009009, doi:https://doi.org/10.1029/2020GC009009 (2020).

66 Keskin, M. Magma generation by slab steepening and breakoff beneath a subduction-accretion complex: An alternative model for collision-related volcanism in Eastern Anatolia, Turkey. *Geophysical Research Letters* **30**, doi:https://doi.org/10.1029/2003GL018019 (2003).

67 Şengör, A. M. C., Özeren, S., Genç, T. & Zor, E. East Anatolian high plateau as a mantle-supported, north-south shortened domal structure. *Geophysical Research Letters* **30**, doi:https://doi.org/10.1029/2003GL017858 (2003).

68 Allen, M. B. & Armstrong, H. A. Arabia–Eurasia collision and the forcing of mid-Cenozoic global cooling. *Palaeogeography, Palaeoclimatology, Palaeoecology* **265**, 52-58, doi:https://doi.org/10.1016/j.palaeo.2008.04.021 (2008).

69 Robertson, A. H. F. *et al.* Tectonic evolution of the South Tethyan ocean: evidence from the Eastern Taurus Mountains (Elaziğ region, SE Turkey). *Geological Society, London, Special Publications* **272**, 231-270, doi:10.1144/gsl.Sp.2007.272.01.14 (2007).

70 Harzhauser, M. *et al.* Biogeographic responses to geodynamics: a key study all around the Oligo–Miocene Tethyan Seaway. *Zoologischer Anzeiger-A Journal of Comparative Zoology* **246**, 241-256 (2007).

71 Rögl, F. Mediterranean and Paratethys. Facts and hypotheses of an Oligocene to Miocene paleogeography (short overview). *Geologica carpathica* **50**, 339-349 (1999).

72 Bialik, O. M., Frank, M., Betzler, C., Zammit, R. & Waldmann, N. D. Two-step closure of the Miocene Indian Ocean Gateway to the Mediterranean. *Scientific Reports* **9**, 8842, doi:10.1038/s41598-019-45308-7 (2019).

73 Segev, A., Avni, Y., Shahar, J. & Wald, R. Late Oligocene and Miocene different seaways to the Red Sea–Gulf of Suez rift and the Gulf of Aqaba–Dead Sea basins. *Earth-Science Reviews* **171**, 196-219, doi:https://doi.org/10.1016/j.earscirev.2017.05.004 (2017).

74 Hernández-Molina, F. J. *et al.* Eocene to middle Miocene contourite deposits in Cyprus: A record of Indian Gateway evolution. *Global and Planetary Change* **219**, 103983, doi:https://doi.org/10.1016/j.gloplacha.2022.103983 (2022).

75 Panza, G. F., Raykova, R. B., Carminati, E. & Doglioni, C. Upper mantle flow in the western Mediterranean. *Earth and Planetary Science Letters* **257**, 200-214, doi:https://doi.org/10.1016/j.epsl.2007.02.032 (2007).

76 Doglioni, C., Carminati, E., Cuffaro, M. & Scrocca, D. Subduction kinematics and dynamic constraints. *Earth-Science Reviews* **83**, 125-175, doi:https://doi.org/10.1016/j.earscirev.2007.04.001 (2007).

77 Wortel, M. J. R. & Spakman, W. Subduction and Slab Detachment in the Mediterranean-Carpathian Region. *Science* **290**, 1910-1917, doi:10.1126/science.290.5498.1910 (2000).

78 Becker, T. W. & Faccenna, C. Mantle conveyor beneath the Tethyan collisional belt. *Earth and Planetary Science Letters* **310**, 453-461, doi:https://doi.org/10.1016/j.epsl.2011.08.021 (2011).

79 Faccenna, C. *et al.* Mantle dynamics in the Mediterranean. *Reviews of Geophysics* **52**, 283-332, doi:https://doi.org/10.1002/2013RG000444 (2014).

80 Hansen, S. E., Nyblade, A. A. & Benoit, M. H. Mantle structure beneath Africa and Arabia from adaptively parameterized P-wave tomography: Implications for the origin of Cenozoic Afro-Arabian tectonism. *Earth and Planetary Science Letters* **319-320**, 23-34, doi:https://doi.org/10.1016/j.epsl.2011.12.023 (2012).

81 Christensen, U. R. The influence of trench migration on slab penetration into the lower mantle. *Earth and Planetary Science Letters* **140**, 27-39, doi:https://doi.org/10.1016/0012-821X(96)00023-4 (1996).

82 Zhong, S. & Gurnis, M. Interaction of weak faults and non-newtonian rheology produces plate tectonics in a 3D model of mantle flow. *Nature* **383**, 245-247, doi:10.1038/383245a0 (1996).

83 Tan, E., Gurnis, M. & Han, L. Slabs in the lower mantle and their modulation of plume formation. *Geochemistry, Geophysics, Geosystems* **3**, 1-24, doi:https://doi.org/10.1029/2001GC000238 (2002).

84 Ricard, Y. & Vigny, C. Mantle dynamics with induced plate tectonics. *Journal of Geophysical Research: Solid Earth* **94**, 17543-17559, doi:https://doi.org/10.1029/JB094iB12p17543 (1989).

85 Hager, B. H. & O'Connell, R. J. A simple global model of plate dynamics and mantle convection. *Journal of Geophysical Research: Solid Earth* **86**, 4843-4867, doi:https://doi.org/10.1029/JB086iB06p04843 (1981).

86 Hager, B. H. & Clayton, R. W. Constraints on the structure of mantle convection using seismic observations, flow models, and the geoid. (1989).

87 Hager, B. H. Subducted slabs and the geoid: Constraints on mantle rheology and flow. *Journal of Geophysical Research: Solid Earth* **89**, 6003-6015, doi:https://doi.org/10.1029/JB089iB07p06003 (1984).

88 Gurnis, M., Mitrovica, J. X., Ritsema, J. & van Heijst, H.-J. Constraining mantle density structure using geological evidence of surface uplift rates: The case of the African Superplume. *Geochemistry, Geophysics, Geosystems* **1**, doi:https://doi.org/10.1029/1999GC000035 (2000).

89 Forte, A. M. *et al.* Joint seismic–geodynamic-mineral physical modelling of African geodynamics: A reconciliation of deep-mantle convection with surface geophysical constraints. *Earth and Planetary Science Letters* **295**, 329-341, doi:https://doi.org/10.1016/j.epsl.2010.03.017 (2010).

90 Richards, M. A. & Hager, B. H. Geoid anomalies in a dynamic Earth. *Journal of Geophysical Research: Solid Earth* **89**, 5987-6002, doi:https://doi.org/10.1029/JB089iB07p05987 (1984).

91 Mitrovica, J. X. & Forte, A. M. New insights obtained from joint inversions for the radial profile of mantle viscosity. *Physics and Chemistry of the Earth* **23**, 857-863, doi:https://doi.org/10.1016/S0079-1946(98)00105-0 (1998).

92 Ricard, Y., Vigny, C. & Froidevaux, C. Mantle heterogeneities, geoid, and plate motion: A Monte Carlo inversion. *Journal of Geophysical Research: Solid Earth* **94**, 13739-13754, doi:https://doi.org/10.1029/JB094iB10p13739 (1989).

93 Tanimoto, T. & Anderson, D. L. Mapping convection in the mantle. *Geophysical Research Letters* **11**, 287-290, doi:https://doi.org/10.1029/GL011i004p00287 (1984).

94 Steinberger, B. & Calderwood, A. R. Models of large-scale viscous flow in the Earth's mantle with constraints from mineral physics and surface observations. *Geophysical Journal International* **167**, 1461-1481, doi:10.1111/j.1365-246X.2006.03131.x (2006).

95 Becker, T. W., Kellogg, J. B., Ekström, G. & O'Connell, R. J. Comparison of azimuthal seismic anisotropy from surface waves and finite strain from global mantle-circulation models. *Geophysical Journal International* **155**, 696-714, doi:10.1046/j.1365-246X.2003.02085.x (2003).

96 Behn, M. D., Conrad, C. P. & Silver, P. G. Detection of upper mantle flow associated with the African Superplume. *Earth and Planetary Science Letters* **224**, 259-274, doi:https://doi.org/10.1016/j.epsl.2004.05.026 (2004).

97 Conrad, C. P. & Behn, M. D. Constraints on lithosphere net rotation and asthenospheric viscosity from global mantle flow models and seismic anisotropy. *Geochemistry, Geophysics, Geosystems* **11** (2010).

98 Becker, T. W. Superweak asthenosphere in light of upper mantle seismic anisotropy. *Geochemistry, Geophysics, Geosystems* **18**, 1986-2003, doi:https://doi.org/10.1002/2017GC006886 (2017).

99 Panasyuk, S. V. & Hager, B. H. A model of transformational superplasticity in the upper mantle. *Geophysical Journal International* **133**, 741-755, doi:10.1046/j.1365-246X.1998.00539.x (1998).

100 Forte, A. M. & Mitrovica, J. X. Deep-mantle high-viscosity flow and thermochemical structure inferred from seismic and geodynamic data. *Nature* **410**, 1049-1056, doi:10.1038/35074000 (2001).

101 Ghosh, A., Becker, T. W. & Zhong, S. J. Effects of lateral viscosity variations on the geoid. *Geophysical Research Letters* **37**, doi:https://doi.org/10.1029/2009GL040426 (2010).

102 Miller, M. S. & Becker, T. W. Mantle flow deflected by interactions between subducted slabs and cratonic keels. *Nature Geoscience* **5**, 726-730, doi:10.1038/ngeo1553 (2012).

103 Yang, T. & Gurnis, M. Dynamic topography, gravity and the role of lateral viscosity variations from inversion of global mantle flow. *Geophysical Journal International* **207**, 1186-1202, doi:10.1093/gji/ggw335 (2016).

104 Mao, W. & Zhong, S. Constraints on Mantle Viscosity From Intermediate-Wavelength Geoid Anomalies in Mantle Convection Models With Plate Motion History. *Journal of Geophysical Research: Solid Earth* **126**, e2020JB021561, doi:https://doi.org/10.1029/2020JB021561 (2021).

105 Becker, T. W. On the effect of temperature and strain-rate dependent viscosity on global mantle flow, net rotation, and plate-driving forces. *Geophysical Journal International* **167**, 943-957, doi:10.1111/j.1365-246X.2006.03172.x (2006).

106 Faccenna, C. & Becker, T. W. Shaping mobile belts by small-scale convection. *Nature* **465**, 602-605, doi:10.1038/nature09064 (2010).

107 Moucha, R. & Forte, A. M. Changes in African topography driven by mantle convection. *Nature Geoscience* **4**, 707-712, doi:10.1038/ngeo1235 (2011).

108 Steinberger, B. & O'Connell, R. J. Changes of the Earth's rotation axis owing to advection of mantle density heterogeneities. *Nature* **387**, 169-173, doi:10.1038/387169a0 (1997).

109 Bunge, H.-P., Hagelberg, C. R. & Travis, B. J. Mantle circulation models with variational data assimilation: inferring past mantle flow and structure from plate motion histories and seismic tomography. *Geophysical Journal International* **152**, 280-301, doi:10.1046/j.1365-246X.2003.01823.x (2003).

110 Conrad, C. P. & Gurnis, M. Seismic tomography, surface uplift, and the breakup of Gondwanaland: Integrating mantle convection backwards in time. *Geochemistry, Geophysics, Geosystems* **4**, doi:https://doi.org/10.1029/2001GC000299 (2003).

111 Colli, L., Bunge, H.-P. & Schuberth, B. S. A. On retrodictions of global mantle flow with assimilated surface velocities. *Geophysical Research Letters* **42**, 8341-8348, doi:https://doi.org/10.1002/2015GL066001 (2015).

112 Ghelichkhan, S., Bunge, H.-P. & Oeser, J. Global mantle flow retrodictions for the early Cenozoic using an adjoint method: evolving dynamic topographies, deep mantle structures, flow trajectories and sublithospheric stresses. *Geophysical Journal International* **226**, 1432-1460, doi:10.1093/gji/ggab108 (2021).

113 Liu, L., Spasojević, S. & Gurnis, M. Reconstructing Farallon Plate Subduction Beneath North America Back to the Late Cretaceous. *Science* **322**, 934-938, doi:doi:10.1126/science.1162921 (2008).

114 Ismail-Zadeh, A., Schubert, G., Tsepelev, I. & Korotkii, A. Inverse problem of thermal convection: numerical approach and application to mantle plume restoration. *Physics of the Earth and Planetary Interiors* **145**, 99-114, doi:https://doi.org/10.1016/j.pepi.2004.03.006 (2004).

115 Müller, R. D. *et al.* A Global Plate Model Including Lithospheric Deformation Along Major Rifts and Orogens Since the Triassic. *Tectonics* **38**, 1884-1907, doi:https://doi.org/10.1029/2018TC005462 (2019).

116 Moucha, R. *et al.* Deep mantle forces and the uplift of the Colorado Plateau. *Geophysical Research Letters* **36**, doi:https://doi.org/10.1029/2009GL039778 (2009).

117 Rowley, D. B. *et al.* Dynamic Topography Change of the Eastern United States Since 3 Million Years Ago. *Science* **340**, 1560-1563, doi:doi:10.1126/science.1229180 (2013).

118 Faccenna, C. *et al.* Role of dynamic topography in sustaining the Nile River over 30 million years. *Nature Geoscience* **12**, 1012-1017, doi:10.1038/s41561-019-0472-x (2019).

119 Le Pichon, X. & Kreemer, C. The Miocene-to-Present Kinematic Evolution of the Eastern Mediterranean and Middle East and Its Implications for Dynamics. *Annual Review of Earth and Planetary Sciences* **38**, 323-351, doi:10.1146/annurev-earth-040809-152419 (2010).

120 Bellahsen, N., Faccenna, C., Funiciello, F., Daniel, J. M. & Jolivet, L. Why did Arabia separate from Africa? Insights from 3-D laboratory experiments. *Earth and Planetary Science Letters* **216**, 365-381, doi:https://doi.org/10.1016/S0012-821X(03)00516-8 (2003).

121 Reilinger, R. & McClusky, S. Nubia–Arabia–Eurasia plate motions and the dynamics of Mediterranean and Middle East tectonics. *Geophysical Journal International* **186**, 971-979, doi:10.1111/j.1365-246X.2011.05133.x (2011).

122 Hafkenscheid, E., Wortel, M. J. R. & Spakman, W. Subduction history of the Tethyan region derived from seismic tomography and tectonic reconstructions. *Journal of Geophysical Research: Solid Earth* **111**, doi:https://doi.org/10.1029/2005JB003791 (2006).

123 Priestley, K. *et al.* New Constraints for the On-Shore Makran Subduction Zone Crustal Structure. *Journal of Geophysical Research: Solid Earth* **127**, e2021JB022942, doi:https://doi.org/10.1029/2021JB022942 (2022).

124 van Hinsbergen, D. J. J., Steinberger, B., Doubrovine, P. V. & Gassmöller, R. Acceleration and deceleration of India-Asia convergence since the Cretaceous: Roles of mantle plumes and continental collision. *Journal of Geophysical Research: Solid Earth* **116**, doi:https://doi.org/10.1029/2010JB008051 (2011).

125 Alvarez, W. Protracted continental collisions argue for continental plates driven by basal traction. *Earth and Planetary Science Letters* **296**, 434-442, doi:https://doi.org/10.1016/j.epsl.2010.05.030 (2010).

126 van der Meer, D. G., van Hinsbergen, D. J. J. & Spakman, W. Atlas of the underworld: Slab remnants in the mantle, their sinking history, and a new outlook on lower mantle viscosity. *Tectonophysics* **723**, 309-448, doi:https://doi.org/10.1016/j.tecto.2017.10.004 (2018).

127 Capitanio, F. A., Faccenna, C. & Funiciello, R. The opening of Sirte basin: Result of slab avalanching? *Earth and Planetary Science Letters* **285**, 210-216, doi:https://doi.org/10.1016/j.epsl.2009.06.019 (2009).

128 van der Meer, D. G., Spakman, W., van Hinsbergen, D. J. J., Amaru, M. L. & Torsvik, T. H. Towards absolute plate motions constrained by lower-mantle slab remnants. *Nature Geoscience* **3**, 36-40, doi:10.1038/ngeo708 (2010).

129 Faccenna, C., Jolivet, L., Piromallo, C. & Morelli, A. Subduction and the depth of convection in the Mediterranean mantle. *Journal of Geophysical Research: Solid Earth* **108**, doi:https://doi.org/10.1029/2001JB001690 (2003).

130 Steinberger, B., Torsvik, T. H. & Becker, T. W. Subduction to the lower mantle – a comparison between geodynamic and tomographic models. *Solid Earth* **3**, 415-432, doi:10.5194/se-3-415-2012 (2012).

131 Peng, D. & Liu, L. Quantifying slab sinking rates using global geodynamic models with data-assimilation. *Earth-Science Reviews* **230**, 104039, doi:https://doi.org/10.1016/j.earscirev.2022.104039 (2022).

132 Rabiee, A., Rossetti, F., Lucci, F. & Lustrino, M. Cenozoic porphyry and other hydrothermal ore deposits along the South Caucasus-West Iranian tectono-magmatic belt: A critical reappraisal of the controlling factors. *Lithos* **430-431**, 106874, doi:https://doi.org/10.1016/j.lithos.2022.106874 (2022).

133 Torsvik, T. H. *et al.* in *Mantle Convection and Surface Expressions* 413-453 (2021).

134 Ricard, Y., Richards, M., Lithgow-Bertelloni, C. & Le Stunff, Y. A geodynamic model of mantle density heterogeneity. *Journal of Geophysical Research: Solid Earth* **98**, 21895-21909, doi:https://doi.org/10.1029/93JB02216 (1993).

135 Shephard, G. E., Liu, L., Müller, R. D. & Gurnis, M. Dynamic topography and anomalously negative residual depth of the Argentine Basin. *Gondwana Research* **22**, 658-663, doi:https://doi.org/10.1016/j.gr.2011.12.005 (2012).

136 Bower, D. J., Gurnis, M. & Flament, N. Assimilating lithosphere and slab history in 4-D Earth models. *Physics of the Earth and Planetary Interiors* **238**, 8-22, doi:https://doi.org/10.1016/j.pepi.2014.10.013 (2015).

137 Steinberger, B. & Torsvik, T. H. A geodynamic model of plumes from the margins of Large Low Shear Velocity Provinces. *Geochemistry, Geophysics, Geosystems* **13**, doi:https://doi.org/10.1029/2011GC003808 (2012).

138 Dannberg, J. & Sobolev, S. V. Low-buoyancy thermochemical plumes resolve controversy of classical mantle plume concept. *Nature Communications* **6**, 6960, doi:10.1038/ncomms7960 (2015).

139 Heyn, B. H., Conrad, C. P. & Trønnes, R. G. How Thermochemical Piles Can (Periodically) Generate Plumes at Their Edges. *Journal of Geophysical Research: Solid Earth* **125**, e2019JB018726, doi:https://doi.org/10.1029/2019JB018726 (2020).

140 Heron, P. J. *et al.* Stranding continental crustal fragments during continent breakup: Mantle suture reactivation in the Nain Province of Eastern Canada. *Geology* **51**, 362-365, doi:10.1130/g50734.1 (2023).

141 Arnould, M., Coltice, N., Flament, N. & Mallard, C. Plate tectonics and mantle controls on plume dynamics. *Earth and Planetary Science Letters* **547**, 116439, doi:https://doi.org/10.1016/j.epsl.2020.116439 (2020).

142 Garfunkel, Z. & Horowitz, A. The upper Tertiary and Quaternary morphology of the Negev, Israel. *Isr. J. Earth Sci* **15**, 101-117 (1966).

143 Zilberman, E. Landscape Evolution in the Central. *Northern, and Northwestern Negev During the Neogene and the Quaternary (Ph. D Thesis, in Hebrew, English abstract), Hebrew University, Jerusalem, Jerusalem*, 164 (1991).

144 Sembroni, A., Molin, P. & Faccenna, C. Drainage system organization after mantle plume impingement: The case of the Horn of Africa. *Earth-Science Reviews* **216**, 103582, doi:https://doi.org/10.1016/j.earscirev.2021.103582 (2021).

145 Gvirtzman, Z. *et al.* Retreating Late Tertiary shorelines in Israel: Implications for the exposure of north Arabia and Levant during Neotethys closure. *Lithosphere* **3**, 95-109, doi:10.1130/l124.1 (2011).

146 Jackson, M. G., Becker, T. W. & Steinberger, B. Spatial Characteristics of Recycled and Primordial Reservoirs in the Deep Mantle. *Geochemistry, Geophysics, Geosystems* **22**, e2020GC009525, doi:https://doi.org/10.1029/2020GC009525 (2021).

147 Steinberger, B., Rathnayake, S. & Kendall, E. The Indian Ocean Geoid Low at a plume-slab overpass. *Tectonophysics* **817**, 229037, doi:https://doi.org/10.1016/j.tecto.2021.229037 (2021).

148 Steinberger, B. Topography caused by mantle density variations: observation-based estimates and models derived from tomography and lithosphere thickness. *Geophysical Journal International* **205**, 604-621 (2016).

149 Schoonman, C. M., White, N. J. & Pritchard, D. Radial viscous fingering of hot asthenosphere within the Icelandic plume beneath the North Atlantic Ocean. *Earth and Planetary Science Letters* **468**, 51-61, doi:https://doi.org/10.1016/j.epsl.2017.03.036 (2017).

150 Sleep, N. H. Hotspots and mantle plumes: Some phenomenology. *Journal of Geophysical Research: Solid Earth* **95**, 6715-6736, doi:https://doi.org/10.1029/JB095iB05p06715 (1990).

151 Nolet, G., Karato, S.-I. & Montelli, R. Plume fluxes from seismic tomography. *Earth and Planetary Science Letters* **248**, 685-699, doi:https://doi.org/10.1016/j.epsl.2006.06.011 (2006).

152 Daradich, A., Mitrovica, J. X., Pysklywec, R. N., Willett, S. D. & Forte, A. M. Mantle flow, dynamic topography, and rift-flank uplift of Arabia. *Geology* **31**, 901-904, doi:10.1130/g19661.1 (2003).

153 Gvirtzman, Z., Faccenna, C. & Becker, T. W. Isostasy, flexure, and dynamic topography. *Tectonophysics* **683**, 255-271, doi:https://doi.org/10.1016/j.tecto.2016.05.041 (2016).

154 Miller, K. G. *et al.* Global Mean and Relative Sea-Level Changes Over the Past 66 Myr: Implications for Early Eocene Ice Sheets. *Earth Science, Systems and Society* **3**, doi:10.3389/esss.2023.10091 (2024).

155 van der Meer, D. G. *et al.* Long-term Phanerozoic global mean sea level: Insights from strontium isotope variations and estimates of continental glaciation. *Gondwana Research* **111**, 103-121, doi:https://doi.org/10.1016/j.gr.2022.07.014 (2022).

156 Miller, K. G. *et al.* Cenozoic sea-level and cryospheric evolution from deep-sea geochemical and continental margin records. *Science Advances* **6**, eaaz1346, doi:10.1126/sciadv.aaz1346 (2020).

157 Barrier, E., Vrielynck, B., Brouillet, J.-F. & Brunet, M.-F. Paleotectonic Reconstruction of the Central Tethyan Realm. Tectonono-Sedimentary-Palinspastic Maps from Late Permian to Pliocene. (2018).

158 Haq, B. U. & Al-Qahtani, A. M. Phanerozoic cycles of sea-level change on the Arabian Platform. *GeoArabia* **10**, 127-160 (2005).

159 Haq, B. U., Hardenbol, J. & Vail, P. R. Chronology of fluctuating sea levels since the Triassic. *Science* **235**, 1156-1167 (1987).

160 Xu, X., Lithgow-Bertelloni, C. & Conrad, C. P. Global reconstructions of Cenozoic seafloor ages: implications for bathymetry and sea level. *Earth and Planetary Science Letters* **243**, 552-564 (2006).

161 Zhang, Z. *et al.* Tropical seaways played a more important role than high latitude seaways in Cenozoic cooling. *Climate of the Past* **7**, 801-813 (2011).

162 Zhu, C., Zhang, Z., Zhu, C. & Zhang, J. Potential Role of Mid-Latitude Seaway on Early Paleogene Atlantic Overturning Circulation. *Geophysical Research Letters* **50**, e2023GL102794, doi:https://doi.org/10.1029/2023GL102794 (2023).

163 Straume, E. O., Nummelin, A., Gaina, C. & Nisancioglu, K. H. Climate transition at the Eocene - Oligocene influenced by bathymetric changes to the Atlantic - Arctic oceanic gateways. *Proceedings of the National Academy of Sciences* **119**, e2115346119, doi:doi:10.1073/pnas.2115346119 (2022).

164 Vahlenkamp, M. *et al.* Ocean and climate response to North Atlantic seaway changes at the onset of long-term Eocene cooling. *Earth and Planetary Science Letters* **498**, 185-195, doi:https://doi.org/10.1016/j.epsl.2018.06.031 (2018).

165 Hutchinson, D. K. *et al.* Arctic closure as a trigger for Atlantic overturning at the Eocene-Oligocene Transition. *Nature Communications* **10**, 3797, doi:10.1038/s41467-019-11828-z (2019).

166 Pillot, Q., Donnadieu, Y., Sarr, A.-C., Ladant, J.-B. & Suchéras-Marx, B. Evolution of Ocean Circulation in the North Atlantic Ocean During the Miocene: Impact of the Greenland Ice Sheet and the Eastern Tethys Seaway. *Paleoceanography and Paleoclimatology* **37**, e2022PA004415, doi:https://doi.org/10.1029/2022PA004415 (2022).

167 Hamon, N., Sepulchre, P., Lefebvre, V. & Ramstein, G. The role of eastern Tethys seaway closure in the Middle Miocene Climatic Transition (ca. 14 Ma). *Clim. Past* **9**, 2687-2702, doi:10.5194/cp-9-2687-2013 (2013).

168 Butzin, M., Lohmann, G. & Bickert, T. Miocene ocean circulation inferred from marine carbon cycle modeling combined with benthic isotope records. *Paleoceanography* **26**, doi:https://doi.org/10.1029/2009PA001901 (2011).

169 Woodruff, F. & Savin, S. M. Miocene deepwater oceanography. *Paleoceanography* **4**, 87-140, doi:10.1029/PA004i001p00087 (1989).

170 Ramsay, A. T., Smart, C. W. & Zachos, J. C. A model of early to middle Miocene deep ocean circulation for the Atlantic and Indian Oceans. *Geological Society, London, Special Publications* **131**, 55-70 (1998).

171 Sarr, A.-C. *et al.* Neogene South Asian monsoon rainfall and wind histories diverged due to topographic effects. *Nature Geoscience* **15**, 314-319, doi:10.1038/s41561-022-00919-0 (2022).

172 Stärz, M., Jokat, W., Knorr, G. & Lohmann, G. Threshold in North Atlantic-Arctic Ocean circulation controlled by the subsidence of the Greenland-Scotland Ridge. *Nature Communications* **8**, 15681, doi:10.1038/ncomms15681 (2017).

173 Maier-Reimer, E., Mikolajewicz, U. & Crowley, T. Ocean General Circulation Model Sensitivity Experiment with an open Central American Isthmus. *Paleoceanography* **5**, 349-366, doi:10.1029/PA005i003p00349 (1990).

174 Sepulchre, P. *et al.* Consequences of shoaling of the Central American Seaway determined from modeling Nd isotopes. *Paleoceanography* **29**, 176-189 (2014).

175 Kennett, J. P. Cenozoic evolution of Antarctic glaciation, the circum-Antarctic Ocean, and their impact on global paleoceanography. *Journal of geophysical research* **82**, 3843-3860 (1977).

176 Sijp, W. P. *et al.* The role of ocean gateways on cooling climate on long time scales. *Global and Planetary Change* **119**, 1-22, doi:http://dx.doi.org/10.1016/j.gloplacha.2014.04.004 (2014).

177 Scher, H. D. *et al.* Onset of Antarctic Circumpolar Current 30 million years ago as Tasmanian Gateway aligned with westerlies. *Nature* **523**, 580-583 (2015).

178 Sauermilch, I. *et al.* Gateway-driven weakening of ocean gyres leads to Southern Ocean cooling. *Nature Communications* **12**, 6465, doi:10.1038/s41467-021-26658-1 (2021).

179 Darin, M. H., Umhoefer, P. J. & Thomson, S. N. Rapid Late Eocene Exhumation of the Sivas Basin (Central Anatolia) Driven by Initial Arabia-Eurasia Collision. *Tectonics* **37**, 3805-3833, doi:https://doi.org/10.1029/2017TC004954 (2018).

180 Licht, A. *et al.* Balkanatolia: The insular mammalian biogeographic province that partly paved the way to the Grande Coupure. *Earth-Science Reviews* **226**, 103929, doi:https://doi.org/10.1016/j.earscirev.2022.103929 (2022).

181 Hönisch, B. *et al.* Toward a Cenozoic history of atmospheric CO2. *Science* **382**, eadi5177, doi:doi:10.1126/science.adi5177 (2023).

182 Palcu, D. V. & Krijgsman, W. The dire straits of Paratethys: gateways to the anoxic giant of Eurasia. *Geological Society, London, Special Publications* **523**, SP523-2021-2073, doi:doi:10.1144/SP523-2021-73 (2022).

183 Ballato, P. *et al.* Multiple Exhumation Phases in the Central Pontides (N Turkey): New Temporal Constraints on Major Geodynamic Changes Associated With the Closure of the Neo-Tethys Ocean. *Tectonics* **37**, 1831-1857, doi:https://doi.org/10.1029/2017TC004808 (2018).

184 Fielding, L. *et al.* The initiation and evolution of the River Nile. *Earth and Planetary Science Letters* **489**, 166-178, doi:https://doi.org/10.1016/j.epsl.2018.02.031 (2018).

185 Jagoutz, O., Macdonald, F. A. & Royden, L. Low-latitude arc–continent collision as a driver for global cooling. *Proceedings of the National Academy of Sciences* **113**, 4935-4940, doi:doi:10.1073/pnas.1523667113 (2016).

186 Rohling, E. J., Marino, G. & Grant, K. M. Mediterranean climate and oceanography, and the periodic development of anoxic events (sapropels). *Earth-Science Reviews* **143**, 62-97, doi:https://doi.org/10.1016/j.earscirev.2015.01.008 (2015).

187 Toumoulin, A. *et al.* Evolution of continental temperature seasonality from the Eocene greenhouse to the Oligocene icehouse –a model–data comparison. *Clim. Past* **18**, 341-362, doi:10.5194/cp-18-341-2022 (2022).

188 Zhang, J. *et al.* Modeling the effects of global cooling and the Tethyan Seaway closure on North African and South Asian climates during the Middle Miocene Climate Transition. *Palaeogeography, Palaeoclimatology, Palaeoecology* **619**, 111541, doi:https://doi.org/10.1016/j.palaeo.2023.111541 (2023).

189 Zhang, Z. *et al.* Aridification of the Sahara desert caused by Tethys Sea shrinkage during the Late Miocene. *Nature* **513**, 401-404, doi:10.1038/nature13705 (2014).

190 Sepulchre, P. *et al.* Tectonic Uplift and Eastern Africa Aridification. *Science* **313**, 1419-1423, doi:doi:10.1126/science.1129158 (2006).

191 Schuster, M. *et al.* The Age of the Sahara Desert. *Science* **311**, 821-821, doi:doi:10.1126/science.1120161 (2006).

192 Bialik, O. M. *et al.* Monsoons, Upwelling, and the Deoxygenation of the Northwestern Indian Ocean in Response to Middle to Late Miocene Global Climatic Shifts. *Paleoceanography and Paleoclimatology* **35**, e2019PA003762, doi:https://doi.org/10.1029/2019PA003762 (2020).

193 Acosta, R. P. & Huber, M. Competing Topographic Mechanisms for the Summer Indo-Asian Monsoon. *Geophysical Research Letters* **47**, e2019GL085112, doi:https://doi.org/10.1029/2019GL085112 (2020).

194 Gheerbrant, E. & Rage, J.-C. Paleobiogeography of Africa: How distinct from Gondwana and Laurasia? *Palaeogeography, Palaeoclimatology, Palaeoecology* **241**, 224-246, doi:https://doi.org/10.1016/j.palaeo.2006.03.016 (2006).

195 Woodburne, M. O. The Great American Biotic Interchange: Dispersals, Tectonics, Climate, Sea Level and Holding Pens. *Journal of Mammalian Evolution* **17**, 245-264, doi:10.1007/s10914-010-9144-8 (2010).

196 Sen, S. Dispersal of African mammals in Eurasia during the Cenozoic: Ways and whys. *Geobios* **46**, 159-172, doi:https://doi.org/10.1016/j.geobios.2012.10.012 (2013).

197 Métais, G., Coster, P., Licht, A., Ocakoğlu, F. & Beard, K. C. Additions to the late Eocene Süngülü mammal fauna in Easternmost Anatolia and the Eocene-Oligocene transition at the periphery of Balkanatolia. *Comptes Rendus. Palevol* **22**, doi:10.5852/cr-palevol2023v22a35 (2023).

198 Stevens, N. J. *et al.* Palaeontological evidence for an Oligocene divergence between Old World monkeys and apes. *Nature* **497**, 611-614, doi:10.1038/nature12161 (2013).

199 Steinthorsdottir, M. *et al.* The Miocene: The Future of the Past. *Paleoceanography and Paleoclimatology* **36**, e2020PA004037, doi:https://doi.org/10.1029/2020PA004037 (2021).

200 Peppe, D. J. *et al.* Oldest evidence of abundant C4 grasses and habitat heterogeneity in eastern Africa. *Science* **380**, 173-177, doi:doi:10.1126/science.abq2834 (2023).

201 Barbolini, N. *et al.* Cenozoic evolution of the steppe-desert biome in Central Asia. *Science Advances* **6**, eabb8227, doi:doi:10.1126/sciadv.abb8227 (2020).

202 Gentis, N. *et al.* Fossil wood from the lower Miocene of Myanmar (Natma Formation): palaeoenvironmental and biogeographic implications. *Geodiversitas* **44**, 853-909, 857 (2022).

203 Hrbek, T. & Meyer, A. Closing of the Tethys Sea and the phylogeny of Eurasian killifishes (Cyprinodontiformes: Cyprinodontidae). *Journal of Evolutionary Biology* **16**, 17-36, doi:https://doi.org/10.1046/j.1420-9101.2003.00475.x (2003).

204 Malaquias, M. A. E. & Reid, D. G. Tethyan vicariance, relictualism and speciation: evidence from a global molecular phylogeny of the opisthobranch genus Bulla. *Journal of Biogeography* **36**, 1760-1777, doi:https://doi.org/10.1111/j.1365-2699.2009.02118.x (2009).

205 Hou, Z. & Li, S. Tethyan changes shaped aquatic diversification. *Biological Reviews* **93**, 874-896, doi:https://doi.org/10.1111/brv.12376 (2018).

206 Wilson, J. T. Did the Atlantic close and then re-open? (1966).

207 Faccenna, C., Becker, T. W., Holt, A. F. & Brun, J. P. Mountain building, mantle convection, and supercontinents: Holmes (1931) revisited. *Earth and Planetary Science Letters* **564**, 116905, doi:https://doi.org/10.1016/j.epsl.2021.116905 (2021).

208 Poblete, F. *et al.* Towards interactive global paleogeographic maps, new reconstructions at 60, 40 and 20 Ma. *Earth-Science Reviews* **214**, 103508, doi:https://doi.org/10.1016/j.earscirev.2021.103508 (2021).

209 Straume, E. O., Gaina, C., Medvedev, S. & Nisancioglu, K. H. Global Cenozoic Paleobathymetry with a focus on the Northern Hemisphere Oceanic Gateways. *Gondwana Research* **86**, 126-143, doi:https://doi.org/10.1016/j.gr.2020.05.011 (2020).

210 Baatsen, M. *et al.* Reconstructing geographical boundary conditions for palaeoclimate modelling during the Cenozoic. *Clim. Past* **12**, 1635-1644, doi:10.5194/cp-12-1635-2016 (2016).

211 Aminov, J., Dupont-Nivet, G., Ruiz, D. & Gailleton, B. Paleogeographic reconstructions using QGIS: Introducing Terra Antiqua plugin and its application to 30 and 50 Ma maps. *Earth-Science Reviews* **240**, 104401, doi:https://doi.org/10.1016/j.earscirev.2023.104401 (2023).

212 Kreemer, C., Blewitt, G. & Klein, E. C. A geodetic plate motion and Global Strain Rate Model. *Geochemistry, Geophysics, Geosystems* **15**, 3849-3889, doi:https://doi.org/10.1002/2014GC005407 (2014).

213 Lu, C., Grand, S. P., Lai, H. & Garnero, E. J. TX2019slab: A New P and S Tomography Model Incorporating Subducting Slabs. *Journal of Geophysical Research: Solid Earth* **124**, 11549-11567, doi:https://doi.org/10.1029/2019JB017448 (2019).

214 Becker, T. W., Lebedev, S. & Long, M. D. On the relationship between azimuthal anisotropy from shear wave splitting and surface wave tomography. *Journal of Geophysical Research: Solid Earth* **117**, doi:https://doi.org/10.1029/2011JB008705 (2012).

215 Torsvik, T. H. *et al.* Pacific-Panthalassic Reconstructions: Overview, Errata and the Way Forward. *Geochemistry, Geophysics, Geosystems* **20**, 3659-3689, doi:https://doi.org/10.1029/2019GC008402 (2019).

216 Kreemer, C. & Chamot-Rooke, N. Contemporary kinematics of the southern Aegean and the Mediterranean Ridge. *Geophysical Journal International* **157**, 1377-1392, doi:10.1111/j.1365-246X.2004.02270.x (2004).

217 Reilinger, R. *et al.* GPS constraints on continental deformation in the Africa-Arabia-Eurasia continental collision zone and implications for the dynamics of plate interactions. *Journal of Geophysical Research: Solid Earth* **111**, doi:https://doi.org/10.1029/2005JB004051 (2006).

218 Husson, L. Dynamic topography above retreating subduction zones. *Geology* **34**, 741-744, doi:10.1130/g22436.1 (2006).

219 Long, M. D. & Becker, T. W. Mantle dynamics and seismic anisotropy. *Earth and Planetary Science Letters* **297**, 341-354, doi:https://doi.org/10.1016/j.epsl.2010.06.036 (2010).

Acknowledgements

EOS acknowledge the support from NRC project 314371 (DOTpaleo). For part of this work EOS was also supported by a Jackson School of Geosciences PLATES-4D Post-Doctoral Scholarship. CF acknowledge discussion with Laurent Jolivet, Paola Molin and Ebru Şengül Uluocak. CF funding support are from Dipartimento di Eccellenza, Scienze, Università Roma TRE. B.S. acknowledges funding from the Innovation Pool of the Helmholtz Association through the Advanced Earth System Modelling Capacity (ESM) activity. TWB was supported partially by NSF EAR 1925939. AL was supported by the European Research Council (ERC) under the European Union's Horizon 2020 research and innovation program (grant agreement No. 101043268).

Competing interests

The authors declare no competing interests.

Author contributions

E.O.S contributed with conceptualization, writing/editing, formal analysis, data curation and visualizations. C.F contributed with conceptualization, writing/editing, and visualization. T.W.B and B.S contributed with conceptualization as well as writing/editing. A.S contributed with writing/editing and data curation. G.Z, A.L, and P.B contributed with writing and editing.

Peer review information

Nature Reviews Earth & Environment thanks [Referee#1 name], [Referee#2 name] and the other, anonymous, reviewer(s) for their contribution to the peer review of this work.

Related links

XXX: https://url

Supplementary information

Supplementary information is available for this paper at https://doi.org/10.1038/s415XX-XXX-XXXX-X

Figures

Figure 1. **Topography, kinematics, and dynamics of the Mediterranean-Tethyan Realm**. **a** | Elevation of the Alpine-Himalaya region, marked with active collisional plate boundaries (bold black line with triangles). The estimated location of the Afar plume is marked with a white circle. Recent volcanics (0-5 Ma; coloured triangles) are obtained by joining together the datasets from refs. [132] and [38], volcanics older than 5 Ma are colored transparent gray. GPS velocities show the tectonic motion relative to Eurasia (purple arrows; data from the compilation of ref.[212]). **b** | Residual topography (data from ref.[148]). **c** | Seismic tomography at 250 km depth (data from TX2019 [213]). Colored arrows show SKS splitting (updated compilation of [214]). This figure shows the correlation between elevation, volcanism, residual topography and seismic tomography.

Figure 2. **Tectonic and geodynamic evolution of the collisional System. a** | Subduction causes subsidence in the overriding Eurasain plate above the slab (blue region). **b** | The plume (orange region) arrives below the African lithosphere and causes uplift and volcanism above. Subducted material penetrates into the lower mantle (slab anchoring), and subsidence in the upper plate continues as the amount of subducted material increases. **c** | The plume-induced uplift could migrate laterally if plume material is entrained by large-scale convection towards the collisional zone. Continental crust arrives in the subduction zone and the trench begins to advance. **d** | Uplift eventually also occurs in the overriding plate, as plume material further migrates laterally, the trench advances further and the slab breaks off. This figure shows the stepwise Cenozoic evolution of the Eastern Mediterranean Tethyan realm.

Figure 3. **Paleogeography and volcanic activity during the Arabia – Eurasia collision a** | Triangles indicate subduction related volcanism while the circles indicate mantle or plume related volcanism. The purple outlined circles and cyan outlined triangles show volcanics dated within +- 1 Myr from the specific time. Orange lines show plate boundaries. Data on volcanism were derived from published studies realized between 1976 and 2023 within the study area (see Supplementary Dataset 1 for the complete list) and by joining together the datasets from refs. [132] and [38]. The panels show how the volcanism migrates northward from East Africa in the Late Eocene, across Arabia, and moving further northward until the present.

Figure 4. **Evolution of paleo-dynamic topography, paleotopography, and mantle cross sections. | a. 50 Ma, b. 40 Ma, c. 30 Ma, d. 20 Ma and e. 10 Ma.** The maps on the left of each panel show paleo-dynamic topography from the results of ref. [9] using TX2019 [213] seismic tomography. The right panels show the paleotopography and mantle density structure along the profiles colored pink in the maps on the left. The latter is computed by backward-advecting present-day density structure inferred from tomography. Profiles are moving with the mantle in the paleomagnetic reference frame of ref. [215]. The modeled dynamic topography anomaly moves northward corresponding to the mantle northward flow seen in the cross section of the mantle density anomalies.

Figure 5. **Ocean circulation and mammal migration during closure of the Tethys Seaway.|** Paleogeography from ref. [9]. Orange arrows indicate mammal migration across the *Gomphotherium* land bridge. Blue arrows show ocean surface flow transport through the Tethys seaway inspired by modeled paleo-ocean circulation of refs. [161,163]. The figure shows the two-step closure of the Tethys Seaway, resulting in the establishment of the *Gomphotherium* land bridge.

Figure 6. **Geodynamic, topographic, climatological, and biogeographical evolution of the Tethys system. a.** Cenozoic atmospheric CO_2 and estimated global mean surface temperature (GMST), from ref. [181]. Major climate intervals are marked for reference: Paleocene – Eocene Thermal Maximum (PETM), Early Eocene Climatic Optimum (EECO), Middle Eocene Climatic Optimum (MECO), Eocene – Oligocene Transition (EOT), Mid Miocene Climatic Optimum (MMCO) and establishment of Antarctic and Northern Hemisphere (NH) ice sheets. **b.** The timing of biogeographic and climatic events. **c.** The width and depth of the oceanic Tethys Seaway and Mesopotamian trough, from the digital elevation models of ref. Straume, et al. [9]. **d.** the northward progression of the positive dynamic topography anomaly (orange line). This anomaly is calculated by extracting the northernmost positive anomaly along the profiles shown in panel **e**. Recorded uplift or subsidence from the Ethiopian, Israel-Jordan, and Anatolia Plateau are shown with triangles, based on data from refs.[33,56,118], compiled by ref.[11]. The triangles color indicates the amount of elevation change. **e.** Regional paleogeographic evolution from 55 Ma to 16 Ma, with profiles showing mantle density anomalies from ref.[9]. Overall, there is a clear correlation between the northward progressing dynamic topography anomaly, the recorded uplift of the Ethiopian, Israel-Jordan, and Anatolia Plateaus, the shallowing and closure of the Seaway, and mammal migrations.

Boxes

BOX1: Present day kinematics and dynamics of the Mediterranean-Tethyan Realm.

Space geodetic techniques provide a detailed picture of the Africa-Arabia-Eurasia system [119,216,217] (Fig. 1a), showing Arabia moving northward at a rate of ~1.5 cm yr-1 relative to Eurasia, much faster than Africa. This movement causes the opening of the Red Sea to the south and colliding to the north. Anatolia moves westward at ~2 cm yr-1 [217], and the Aegean region moves even faster at ~3.3 cm yr-1 south towards the retreating Hellenic trench[216,217]. This pattern generates a large, anti-clockwise circuit with a pole of rotation around the Nile Delta [119] (Fig. 1a).

Residual topography estimates show elongated positive anomalies, with a large bulge over the Ethiopian plateau, following the eastern shoulder of the Red Sea, and extending northward toward northwest Arabia [37,107,152,153] (Fig. 1b). By construction, these topographic anomalies are not isostatically supported and can be compared with seismic tomography (Fig. 1c). Both positive and negative residual topography anomalies correspond to low and high seismic velocity anomalies in the upper mantle, respectively. This correlation suggests that the thermal structure of the mantle and the associated radial convection patterns, with hot upwellings and cold downwellings, are influencing surface topography[37,78,89,106,107,152,218].

Horizontal mantle flow can be deduced from *SKS* splitting inferences of seismic anisotropy, sensitive to the orientation of deformation in upper mantle flow[37,80,219]. The *SKS* "fast axes" align with shear to first order and thus indicate a northerly flow trend in the region, following the positive residual topography and then turn to a northeasterly direction below Anatolia and Iran (Fig. 1c). Mantle flow therefore likely contribute to higher elevations from Afar toward northwest Arabia at present, and past convective effects were also likely relevant, including for the Arabia-Eurasia collision and closure of the Tethys Seaway.

Fig 1

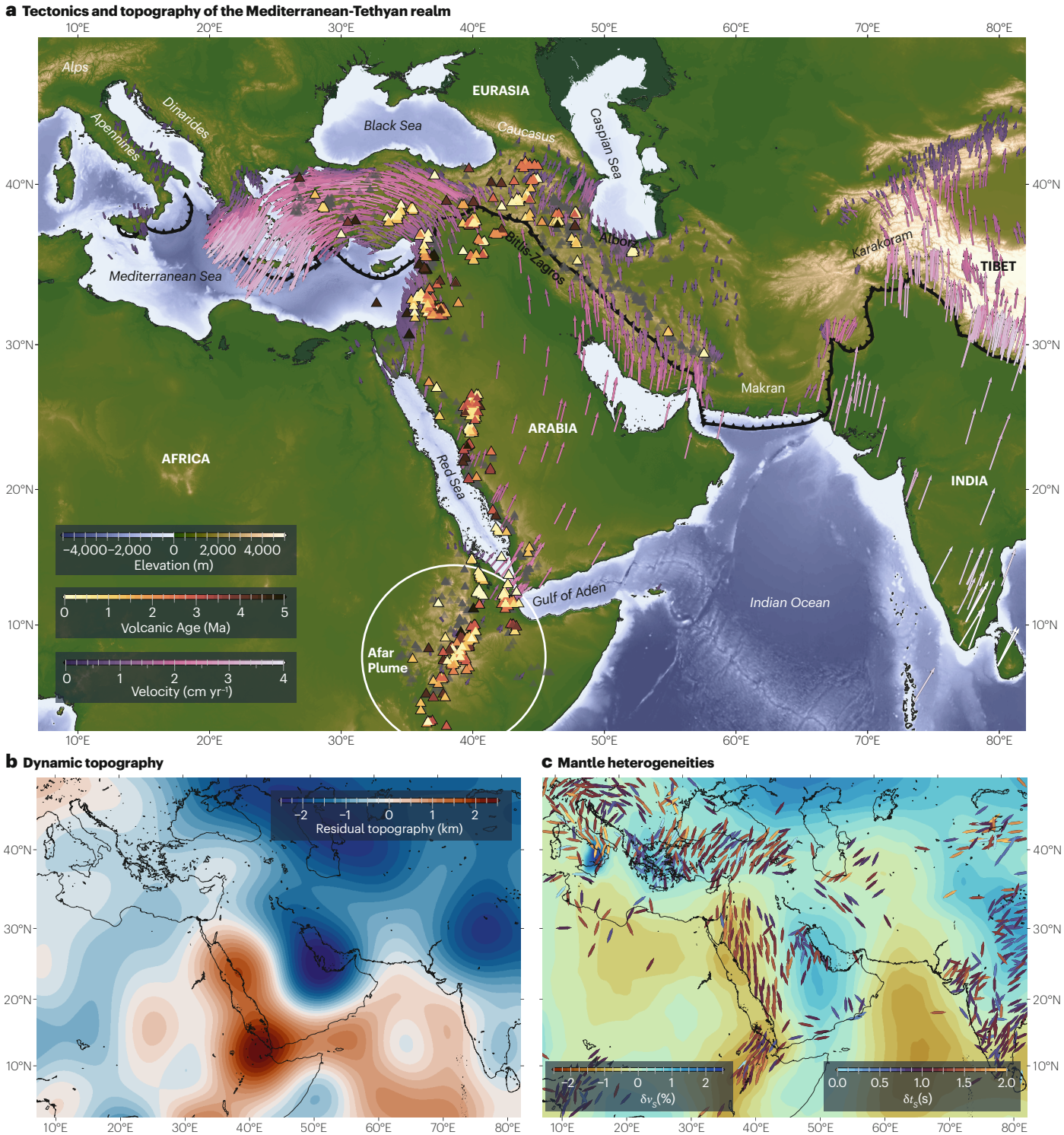
a Tectonics and topography of the Mediterranean-Tethyan realm
Alps
Dinarides
Apennines
EURASIA
Black Sea
Caucasus
Caspian Sea
Mediterranean Sea
Bitlis-Zagros
Alborz
Karakoram
TIBET
Makran
ARABIA
AFRICA
Red Sea
INDIA
Gulf of Aden
Indian Ocean
Afar Plume
−4,000 −2,000 0 2,000 4,000
Elevation (m)
0 1 2 3 4 5
Volcanic Age (Ma)
0 1 2 3 4
Velocity (cm yr⁻¹)
10°E 20°E 30°E 40°E 50°E 60°E 70°E 80°E
40°N 30°N 20°N 10°N
b Dynamic topography
−2 −1 0 1 2
Residual topography (km)
c Mantle heterogeneities
−2 −1 0 1 2
δvS(%)
0.0 0.5 1.0 1.5 2.0
δtS(s)

Fig 2

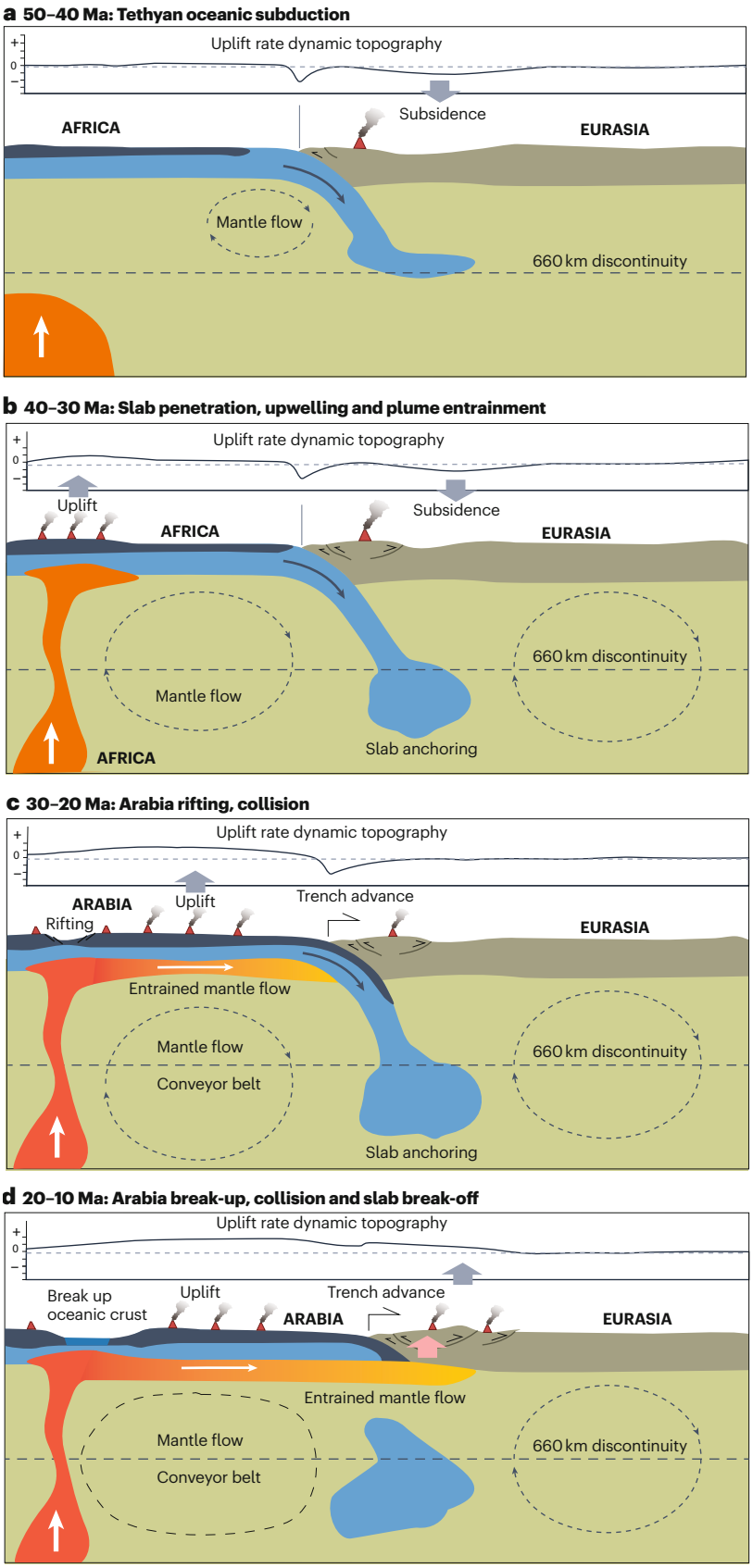
a 50–40 Ma: Tethyan oceanic subduction
Uplift rate dynamic topography
+
0
–
Subsidence
AFRICA
EURASIA
Mantle flow
660 km discontinuity
b 40–30 Ma: Slab penetration, upwelling and plume entrainment
Uplift rate dynamic topography
Uplift
Subsidence
AFRICA
EURASIA
660 km discontinuity
Mantle flow
Slab anchoring
AFRICA
c 30–20 Ma: Arabia rifting, collision
Uplift rate dynamic topography
ARABIA
Rifting
Uplift
Trench advance
EURASIA
Entrained mantle flow
Mantle flow
Conveyor belt
660 km discontinuity
Slab anchoring
d 20–10 Ma: Arabia break-up, collision and slab break-off
Uplift rate dynamic topography
Break up
oceanic crust
Uplift
Trench advance
ARABIA
EURASIA
Entrained mantle flow
Mantle flow
Conveyor belt
660 km discontinuity

Fig 3

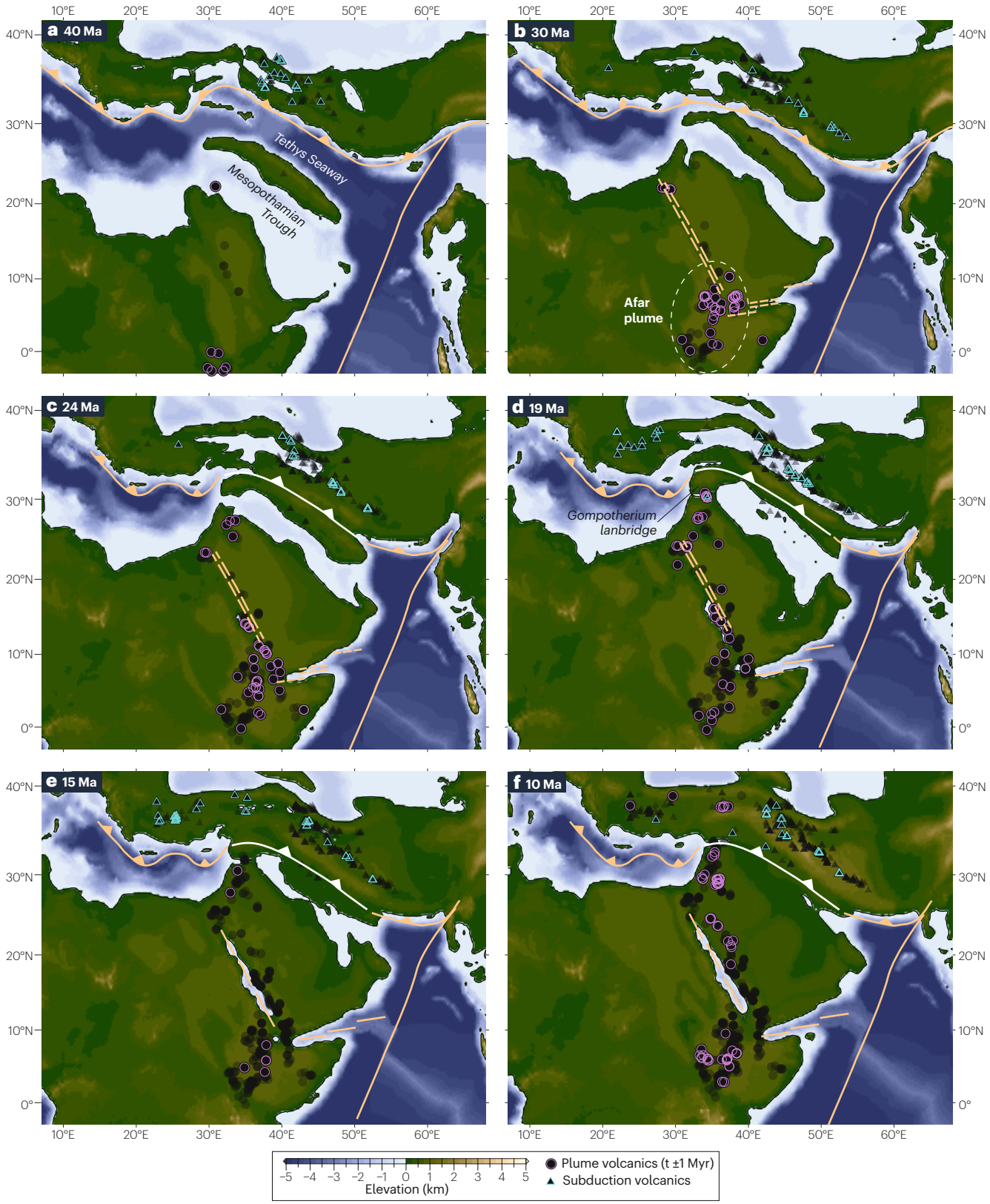
a 40 Ma
Tethys Seaway
Mesopothamian Trough
b 30 Ma
Afar plume
c 24 Ma
d 19 Ma
Gompotherium lanbridge
e 15 Ma
f 10 Ma
10°E
20°E
30°E
40°E
50°E
60°E
40°N
30°N
20°N
10°N
0°
−5 −4 −3 −2 −1 0 1 2 3 4 5
Elevation (km)
Plume volcanics (t ±1 Myr)
Subduction volcanics

Fig 4

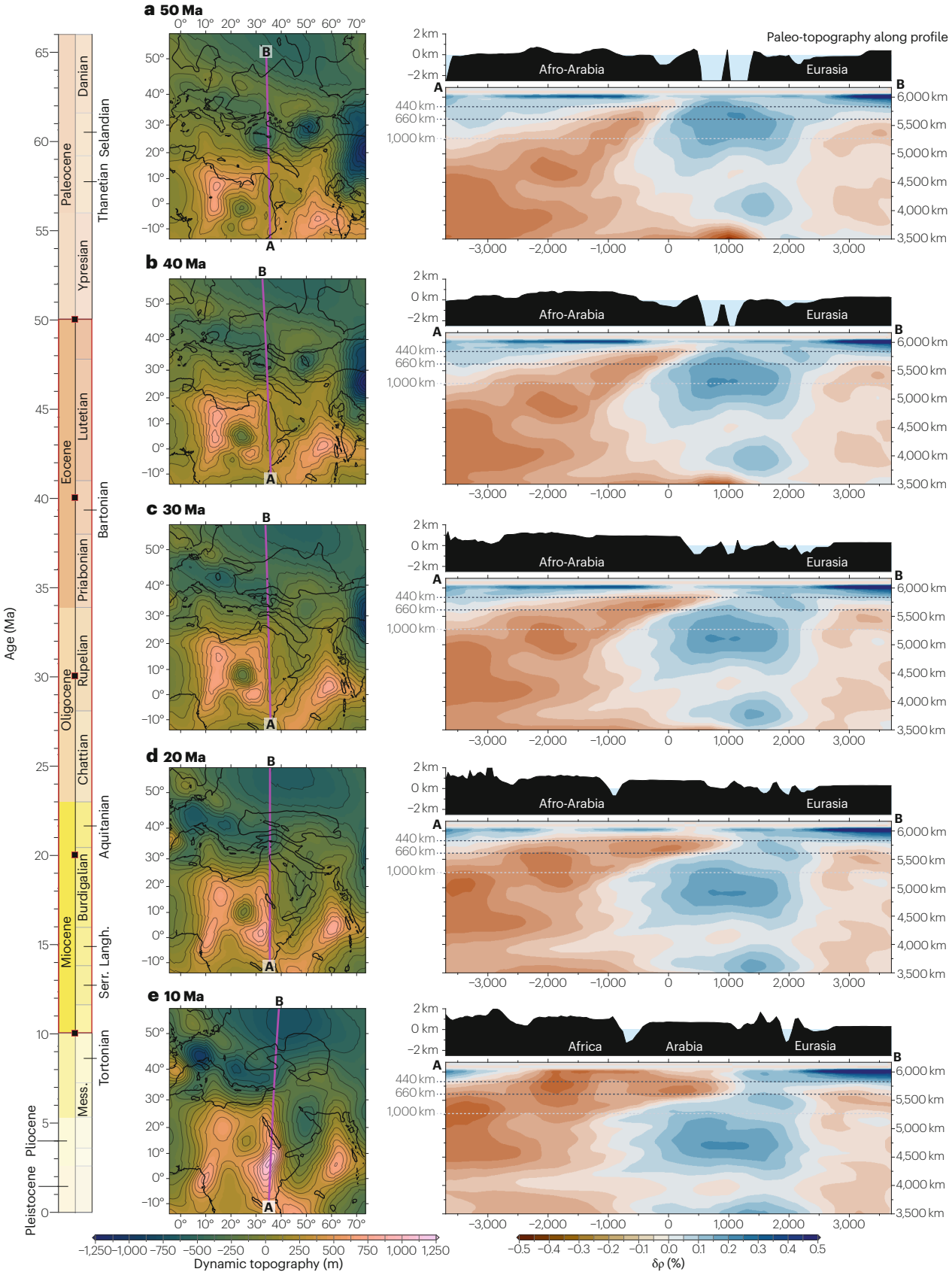
a 50 Ma
b 40 Ma
c 30 Ma
d 20 Ma
e 10 Ma
Paleo-topography along profile
Afro-Arabia
Eurasia
Africa
Arabia
Age (Ma)
Paleocene
Eocene
Oligocene
Miocene
Pliocene
Pleistocene
Danian
Selandian
Thanetian
Ypresian
Lutetian
Bartonian
Priabonian
Rupelian
Chattian
Aquitanian
Burdigalian
Serr.
Langh.
Tortonian
Mess.
Dynamic topography (m)
δρ (%)

Fig 5

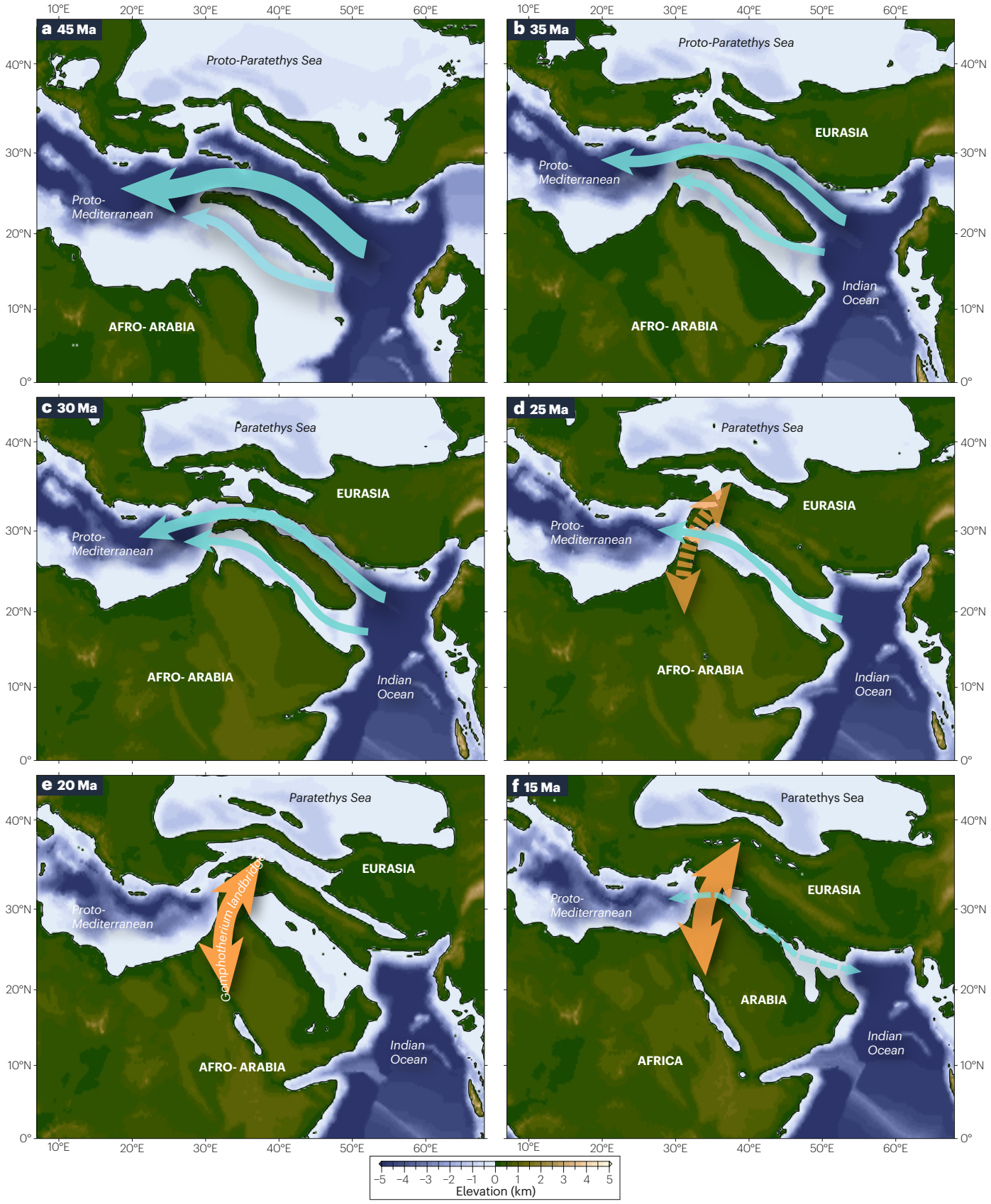
a 45 Ma
Proto-Paratethys Sea
Proto-Mediterranean
AFRO- ARABIA
b 35 Ma
Proto-Paratethys Sea
EURASIA
Proto-Mediterranean
Indian Ocean
AFRO- ARABIA
c 30 Ma
Paratethys Sea
EURASIA
Proto-Mediterranean
AFRO- ARABIA
Indian Ocean
d 25 Ma
Paratethys Sea
EURASIA
Proto-Mediterranean
AFRO- ARABIA
Indian Ocean
e 20 Ma
Paratethys Sea
EURASIA
Proto-Mediterranean
Gomphotherium landbridge
AFRO- ARABIA
Indian Ocean
f 15 Ma
Paratethys Sea
EURASIA
Proto-Mediterranean
ARABIA
AFRICA
Indian Ocean
10°E 20°E 30°E 40°E 50°E 60°E
0° 10°N 20°N 30°N 40°N
−5 −4 −3 −2 −1 0 1 2 3 4 5
Elevation (km)

Fig 6

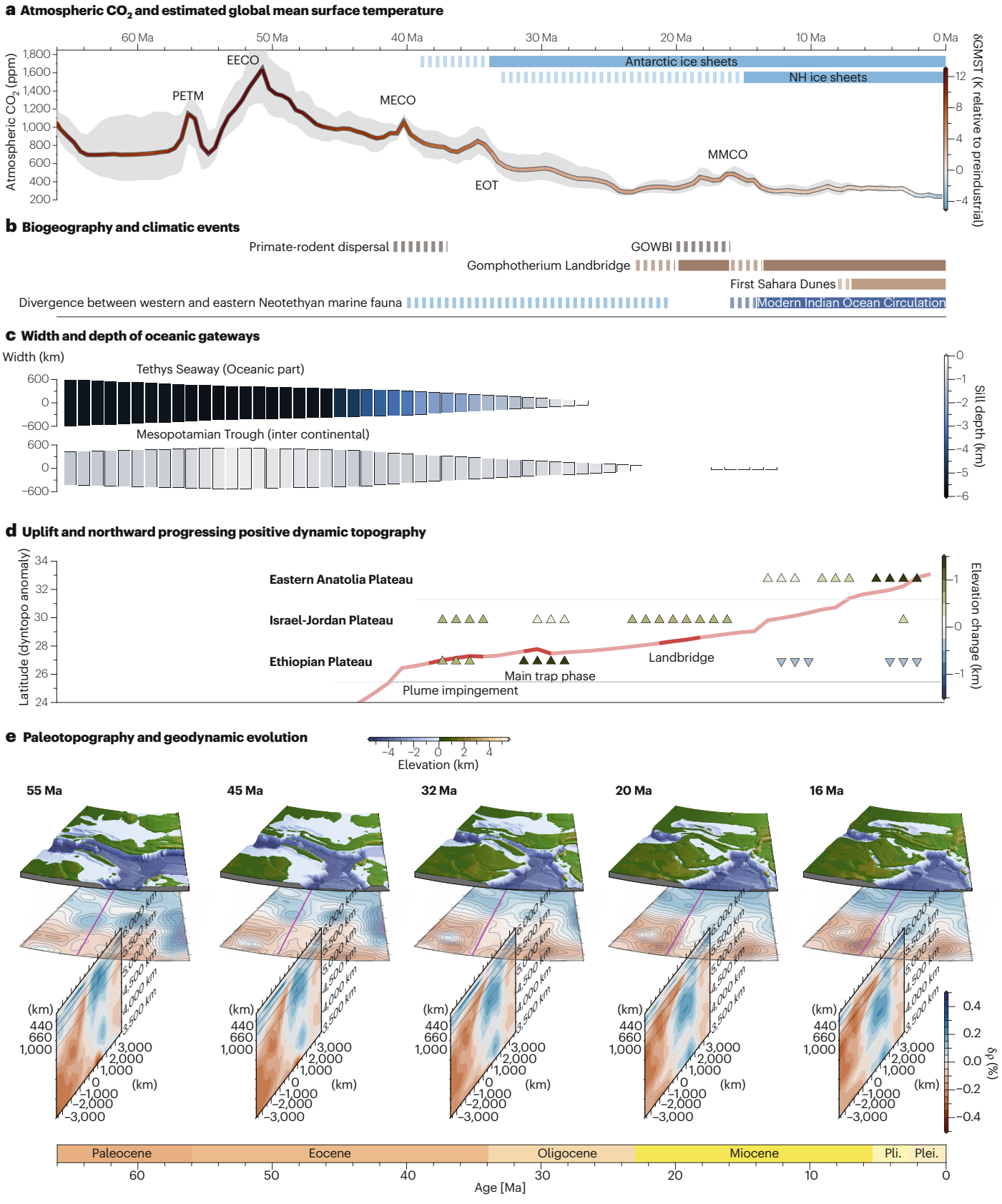
a Atmospheric CO2 and estimated global mean surface temperature
60 Ma
50 Ma
40 Ma
30 Ma
20 Ma
10 Ma
0 Ma
Atmospheric CO2 (ppm)
1,800
1,600
1,400
1,200
1,000
800
600
400
200
EECO
PETM
MECO
EOT
MMCO
Antarctic ice sheets
NH ice sheets
δGMST (K relative to preindustrial)
12
8
4
0
−4
b Biogeography and climatic events
Primate-rodent dispersal
GOWBI
Gomphotherium Landbridge
First Sahara Dunes
Divergence between western and eastern Neotethyan marine fauna
Modern Indian Ocean Circulation
c Width and depth of oceanic gateways
Width (km)
Tethys Seaway (Oceanic part)
600
0
−600
Mesopotamian Trough (inter continental)
600
0
−600
Sill depth (km)
0
−1
−2
−3
−4
−5
−6
d Uplift and northward progressing positive dynamic topography
Latitude (dyntopo anomaly)
34
32
30
28
26
24
Eastern Anatolia Plateau
Israel-Jordan Plateau
Ethiopian Plateau
Landbridge
Main trap phase
Plume impingement
Elevation change (km)
1
0
−1
e Paleotopography and geodynamic evolution
−4 −2 0 2 4
Elevation (km)
55 Ma
45 Ma
32 Ma
20 Ma
16 Ma
(km)
440
660
1,000
3,000
2,000
1,000
0
−1,000
−2,000
−3,000
(km)
δρ (%)
0.4
0.2
0.0
−0.2
−0.4
Paleocene
Eocene
Oligocene
Miocene
Pli.
Plei.
60
50
40
30
20
10
0
Age [Ma]